Structures 80 (2025) 109929

Contents lists available at ScienceDirect

Structures

journal homepage: www.elsevier.com/locate/structures

A design-oriented solution for FRP-to-substrate bonded joints with a transversely compressed mechanical end anchorage

Hugo C. Biscaia [a,b,*], Cristina Barris [c], Jian-Guo Dai [d]

[a] UNIDEMI, Department of Mechanical and Industrial Engineering, NOVA School of Science and Technology, Caparica 2829-516, Portugal
[b] Laboratório Associado de Sistemas Inteligentes, LASI, Guimarães 4800-058, Portugal
[c] AMADE, Polytechnic School, University of Girona, Girona 17003, Spain
[d] Department of Architecture and Civil Engineering, City University of Hong Kong, Hong Kong, China

ARTICLE INFO

Keywords:
FRP composites
Analytical model
FRP-to-substrate joints
Debonding
End anchorages
Pull-push test

ABSTRACT

The strengthening of damaged concrete, steel or timber beams with carbon fibre-reinforced polymers (CFRP) has increased continuously. Usually, the CFRP composite is externally bonded (EB) to the soffit of the beam, and the adhesion between both surfaces is critical for the success of this strengthening technique. The FRP-to-substrate interfaces are prone to debond prematurely, so to delay or prevent this, additional anchorages are used. However, the performance of mechanically anchored FRP-to-substrate joints remains unclear due to the high diversity of existing anchorage systems. To mitigate this gap, an analytical model is developed to simulate the influence of a transversely compressed mechanical end anchorage on CFRP-to-substrate joints. The analytical model replaces the mechanical end anchorage with a nonlinear spring. A series of different generated cases is considered and simulated by the analytical model and validated by the Finite Element Method (FEM). Experimental data found in the literature are also simulated using the analytical model. The results showed that the transversely compressed end anchorage is efficient when a long anchorage is used rather than a shorter one. The analytical model can also predict the nonlinear load increment of the anchored bonded joints as experimentally reported in the literature.

1. Introduction

Fibre-reinforced polymers (FRP) such as carbon (C)FRP have been used widely in the strengthening of damaged concrete, steel or timber structures, forming adhesively bonded structures. Compared to other traditional materials such as mild steel or stainless steel, CFRP composites have a good strength-to-weight ratio and good durability [1–5].

CFRP composites are usually post-installed on the soffit of damaged structures through the externally bonded reinforcement (EBR) or other bonding techniques such as the EBR on grooves (EBROG) [6–8] or in grooves (EBRIG) [8–10], or near-surface mounted [11–14]. However, it is known that CFRP composites prematurely debond from the substrate, i.e., at a low strain value compared to their rupture strain values. To overcome this issue, the use of the continuous reinforcement embedded at ends (CREatE) is effective as it prevents the premature debonding of the CFRP from the substrate and, at the same time, it can improve the shear strength of the beam [15–17]. Normally, the addition of steel end anchorages to the EBR system is much easier to implement. Other anchorage types have been used and studied by several researchers, such as CFRP spike anchors [18–21], CFRP wrapping [22–25], increased CFRP width [26,27], steel anchors with washers [28,29], and steel plates [30–33], among others.

The rationale for using CFRP spike anchors is to transfer the loads into the core of the concrete and increase the strength of the CFRP-to-concrete bonded joints. However, the spike anchors tend to rupture when subjected to shear forces. The strength of the CFRP-to-concrete joints tends to increase with the number of CFRP spike anchors; however, to the best of the authors' knowledge, there is a lack of design guidelines or comprehensive recommendations available in the literature. Therefore, the optimal number of spike anchors to be used or the ideal distance between them remains poorly understood. For obvious reasons, using these anchors on steel structures is not advised, and their use is limited to concrete or timber structures.

By wrapping the CFRP composite with more CFRP composites, the

* Corresponding author at: UNIDEMI, Department of Mechanical and Industrial Engineering, NOVA School of Science and Technology, Caparica 2829-516, Portugal.
E-mail address: hb@fct.unl.pt (H.C. Biscaia).

https://doi.org/10.1016/j.istruc.2025.109929
Received 8 April 2025; Received in revised form 1 July 2025; Accepted 10 August 2025
Available online 16 August 2025

width of the CFRP-to-substrate system increases and the interfacial slips of these wrapped areas are reduced. Since the strength of the CFRP-to-substrate bonded joints increases linearly with the width of the CFRP composite [34–38], the CFRP wrap aims to enhance the ultimate strength of the CFRP-to-substrate bonded joint. However, if the CFRP wrapping area slips, the efficiency of this end anchorage is lost. To prevent such a scenario, air voids in the wrapping area should be avoided, and the preferred direction of the fibres should be the same as the load direction of the CFRP-to-concrete joint. This anchorage technique is also easier to implement in simple substrate geometries, such as the rectangular cross-sectional area of beams. However, the corners of the substrate should be smoothed so that stress concentrations in those regions can be avoided.

Using a steel plate as an end anchorage of CFRP-to-substrate bonded joints is a well-accepted solution among researchers, e.g. [33,39–43]. The steel plate is externally pressed against the CFRP composite and fixed to the substrate through steel bolts. The aim of transversely compressing the CFRP-to-substrate bonded joints is to improve the local adherence between adherends by increasing the maximum shear bond stress developed within the interface and promoting friction between the CFRP and the substrate after its debonding. Therefore, the friction angle of the CFRP-to-substrate bonded joint and the compressive stress applied to the steel plate contribute to the improvement of the ultimate strength of the joint [44–46], and they must be well-defined. However, defining them correctly requires experimental studies. For instance, an exaggerated compression of the steel plate against the CFRP composite may lead to the rupture of the carbon fibres, and a low compression magnitude may lead to the slip of CFRP beneath the anchorage and, consequently, lead to an inefficient mechanical end anchorage. With all these concerns in mind, Biscaia and Chastre [46] have proposed two design methods for using transversely compressed end anchorages. One is more complex than the other, resulting in more conservative values. Still, in the two methods, the debonding process of transversely compressed CFRP-to-substrate bonded joints was investigated through advanced numerical models, which do not facilitate fast and rational decisions for engineers or practitioners. To help with the decision, design, and understanding of the bond behaviour of transversely compressed end anchorages of CFRP-to-substrate joints, the use of analytical solutions rather than advanced numerical modelling will be more helpful to everyone and they may potentially to be included in standards or codes in the future, promoting, therefore, the more rational, economical and widespread use of these bonding systems.

Aligned with these thoughts and the urgent need for clarification on these subjects, an analytical solution for transversely compressed end anchorages of FRP-to-substrate joints has been developed. The analytical model is based on a well-known exponential bond-slip relationship [47], which can be used for several FRP-to-substrate bonded joints under different conditions. In the case of the presence of a transversely compressed mechanical end anchorage, only the strain-slip (or load-slip) relationship of the end anchorage needs to be known. To that end, the end anchorage is replaced by a nonlinear axial spring with the same load-slip (or strain-slip) behaviour as the transversely compressed end anchorage. In cases where this strain-slip relationship is unknown, two numerical models were assumed to predict the strain-slip relationship of the transversely compressed end anchorage.

The analytical model can also predict the complete load-slip response of the FRP-to-substrate bonded joints with or without an end anchorage, as well as the slips, shear bond stresses and FRP strains developed throughout the bonded length (see Fig. 1a). However, it is limited to those cases where the bond-slip relationship shows a final friction stress developed within the FRP and the substrate interface (see Figs. 1b or 1c).

The validation of the analytical model was carried out by comparing the results with those obtained from the numerical simulations of twenty-five different specimens with the Finite Element Method (FEM). In addition, three other studies available in the literature [48–50] were simulated by the analytical model. Due to the lack of available experimental data in the literature, some other cases were extrapolated from the experiments in those cited studies. Despite its simplicity, the analytical model covered a wide range of FRP-to-substrate scenarios, proving its high level of versatility when compared with other existing analytical models. Moreover, its attested accuracy in alignment with both FEM analysis and experimental results makes the analytical model a valuable and straightforward design tool for engineers, practitioners and researchers worldwide.

2. Theoretical framework

In this section, comprehensive descriptions of all derivations of the analytical model are presented, as well as all their key assumptions. The advantages and limitations of the analytical model are also identified.

2.1. Analytical model

Before starting the description of the analytical model, it is essential to establish its initial assumptions. The analytical model aims to simulate the full debonding process of a wide range of scenarios involving FRP composites EB to a substrate with a transversely compressed end anchorage. The analytical model is developed upon the following key assumptions:

(i) the thickness of the adherends (FRP and substrate) remains constant during the debonding process;

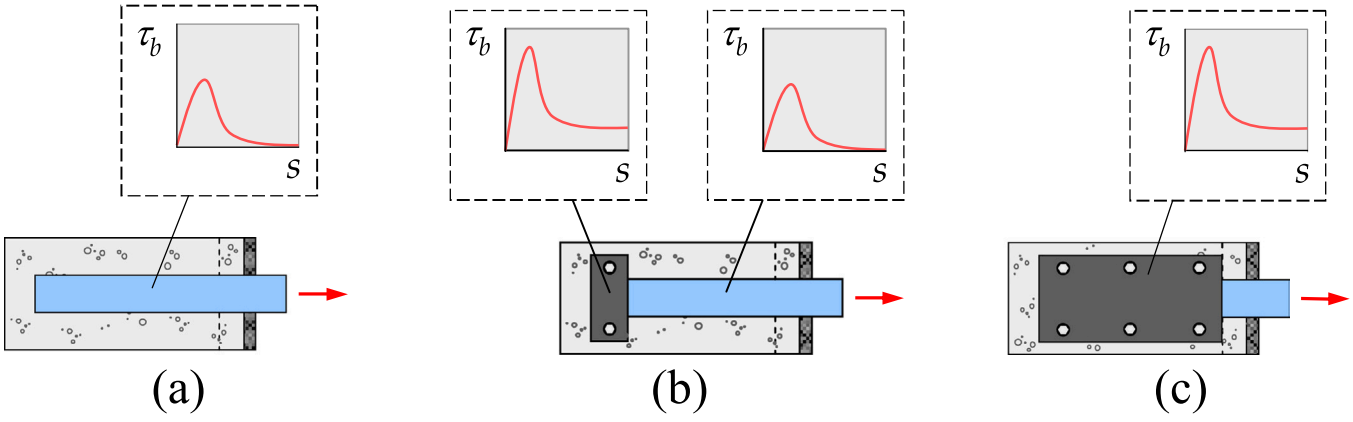

Fig. 1. Examples of FRP-to-substrate bonded joints: (a) without anchorages (covered by the analytical model); (b) with a transversely compressed end anchorage (covered by the analytical model); and (c) fully under a transversely compressed mechanical anchorage (not covered by the analytical model).

(ii) the adherends exhibit linear elastic behaviour during the full debonding process of the joint;
(iii) normal bond stresses, i.e., perpendicularly developed to the bonded area, are ignored;
(iv) the interface between the FRP composite and the substrate (including the adhesive layer) is represented by a no-thickness cohesive zone model (CZM), whose behaviour under Mode II loading is characterised by a local bond-slip relationship (e.g., [51–53]);
(v) the shear bond stresses are uniformly distributed across the width of the FRP composite;
(vi) the transversely compressed end anchorage exhibits a nonlinear behaviour, modelled by a nonlinear spring as shown in Fig. 2. The load-slip curve (i.e., F_0-s_0) of this anchorage is defined according to:

$$F_0 = k(s)\cdot s_0 \tag{1}$$

where s_0 is the slip at the tip of the end anchorage; and $k(s)$ is the nonlinear stiffness of the end anchorage given by its load-slip curve. It should be noted that the length of the end anchorage, the compressive stress magnitude or the value of the friction between adherends are not reflected in Eq. (1), but the debonding of the FRP composite from the substrate is always consistent with pure fracture Mode II. So, the bending of the FRP composite is not considered and only axial deformations of the adherends are assumed.

Under the previously mentioned key assumptions, the equation that governs the debonding process of the FRP composite from the substrate is defined according to the following known 2nd-order differential equation [34,54–59]:

$$\frac{d^2 s}{dx^2} - \lambda\cdot\tau_b(s) = 0 \tag{2}$$

where τ_b is the shear bond stress developed in the interface between the FRP composite and the substrate; s is the slip of the FRP-to-substrate interface; x is the longitudinal coordinate parallel with the bonded length of the joint with origin at the nonlinear spring (see Fig. 2); and λ is given by

$$\lambda = \frac{1}{E_r\cdot t_r} + \frac{1}{E_s\cdot t_s}\cdot\frac{b_r}{b_s} \tag{3}$$

where E_r and E_s are the elastic moduli of the FRP composite and substrate, respectively; t_r and t_s are the thicknesses of the FRP composite and substrate, respectively; and b_r and b_s are the widths of the FRP composite and substrate, respectively.

To find the solution of Eq. (2) it is necessary to know the local bond behaviour between adherends, i.e., $\tau_b(s)$, which varies depending, e.g., on the type of adherends [60], adhesive type [61–63], bonding technique [64] or even on the stresses perpendicularly developed to the bonded area [44–46]. Thus, the bond-slip relationship is different and it is usually defined through different mathematical functions that correlate the interfacial slips with the shear bond stresses developed in the interface [45,47,63–69]. In the present work, the well-known exponential bond-slip relationship originally proposed by Dai et al. [47] is considered due to its versatility to integrate or differentiate, facilitating the determination of the analytical solution of Eq. (2) [45,47]. With only one expression, this exponential bond-slip relationship can describe the following stages of an FRP-to-substrate bonded joint: Elastic (E), Softening (S), and Debonding (D). These stages are usually observed on CFRP-to-concrete [70–74], steel [75–77], or masonry [78,79] bonded joints subjected to pull-pull or pull-push tests. It should be noted also that the exponential bond-slip relationship proposed by Dai et al. [47] assumes no friction stresses developed in the FRP-to-substrate interface, and after the S stage, no shear bond stresses develop in the interface, i.e., there is no interaction between the adherends.

The derivation of the exponential bond-slip relationship is briefly explained next. Thus, to obtain the exponential bond-slip relationship, the experimental strain-slip relationship is approximated through the following equation:

$$\varepsilon_r = \varepsilon_{r\,\max}\cdot\left(1 - e^{-B\cdot s}\right) \tag{4}$$

where $\varepsilon_{r\max}$ is the maximum strain developed in the FRP composite; and B is the stiffness index of the interface, which is obtained by fitting Eq. (4) with the experimental data [47]. Considering the equilibrium of a finite length dx of the FRP-to-substrate bonded joint, the following expression can be obtained:

$$\tau_b = E_r\cdot t_r\cdot\frac{d\varepsilon_r}{dx} = E_r\cdot t_r\cdot\frac{d\varepsilon_r}{ds}\cdot\frac{ds}{dx} \tag{5}$$

Introducing the derivative with respect to x of Eq. (4) in Eq. (5), yields:

$$\tau_b = E_r\cdot t_r\cdot\varepsilon_{r\,\max}{}^2\cdot B\cdot e^{-B\cdot s}\cdot\left(1 - e^{-B\cdot s}\right) \tag{6}$$

From the integration of Eq. (6) with respect to s, the Mode II fracture energy is

$$G_F = \frac{E_r\cdot t_r\cdot\varepsilon_{r\,\max}{}^2}{2} \tag{7}$$

and Eq. (7) can be rewritten as

$$\tau_b = 2B\cdot G_F\cdot\left(e^{-B\cdot s} - e^{-2B\cdot s}\right) \tag{8}$$

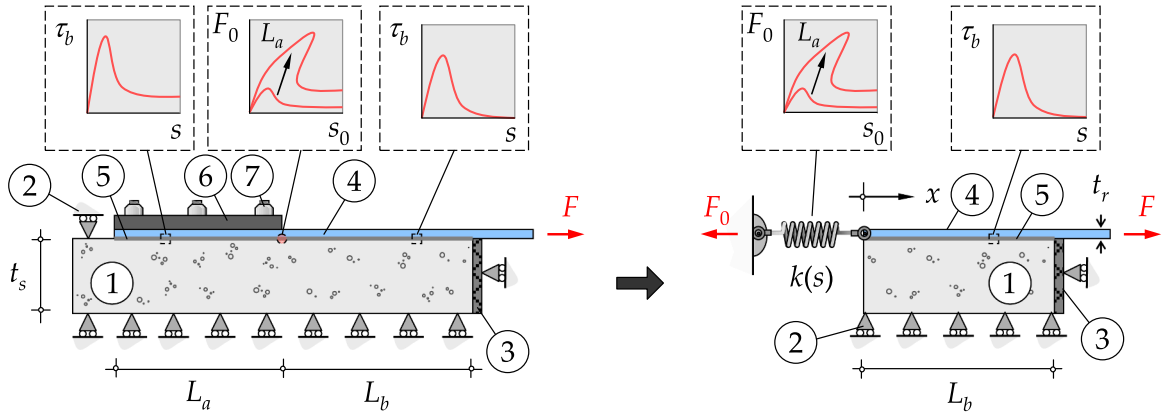

Key: 1 – Substrate; 2 – Roller support; 3 – Steel reaction plate; 4 – FRP composite; 5 – Adhesive; 6 – Steel plate; 7 – Steel bolt.

Fig. 2. FRP-to-substrate joints with a transversely compressed end anchorage and its idealised joint.

The maximum shear bond stress developed in the FRP-to-substrate interface can be determined by writing the first derivative of Eq. (8) with respect to s and equating it to zero. Thus, the slip corresponding to the maximum shear bond stress is found, i.e.,

$$s_{\max} = \frac{\ln(2)}{B} \tag{9}$$

Denoting $\tau_{b,\max 0}$ as the maximum shear bond stress under pure fracture Mode II (i.e., free of any normal bond stresses), introducing Eq. (9) in Eq. (8), this bond stress can be defined as

$$\tau_{b,\ \max\ 0} = \frac{B \cdot G_F}{2} \tag{10}$$

Introducing Eq. (8) in Eq. (2), the governing equation of the debonding process is defined as:

$$\frac{d^2 s}{dx^2} - 2\lambda \cdot B \cdot G_F \cdot \left(e^{-B \cdot s} - e^{-2B \cdot s}\right) = 0 \tag{11}$$

Since

$$\frac{d^2 s}{dx^2} = \frac{d}{dx}\left(\frac{ds}{dx}\right) = \frac{d}{ds}\left(\frac{ds}{dx}\right)\frac{ds}{dx} = \frac{1}{2}\cdot\frac{d}{ds}\left(\frac{ds}{dx}\right)^2 \tag{12}$$

Eq. (11) can be rewritten according to

$$\left(\frac{ds}{dx}\right)^2 = \int 4\lambda \cdot B \cdot G_F \cdot \left(e^{-B \cdot s} - e^{-2B \cdot s}\right) ds \tag{13}$$

Bearing in mind that

$$2B \cdot \left(e^{-B \cdot s} - e^{-2B \cdot s}\right) = \frac{d}{ds}\left(1 - e^{-B \cdot s}\right)^2 \tag{14}$$

Eq. (13) can be rewritten as

$$\left(\frac{ds}{dx}\right)^2 = 2\lambda \int G_F \cdot \frac{d}{ds}\left(1 - e^{-B \cdot s}\right)^2 ds \tag{15}$$

Integrating Eq. (15) leads to:

$$\frac{ds}{dx} = \sqrt{2\lambda \cdot G_F \cdot \left(1 - e^{-B \cdot s}\right)^2 + C_1} \tag{16}$$

where C_1 is a constant to be found from the strains developed at the FRP composite free end (ε_{r0}), i.e., at $x = 0$. To that end, the general expression originally proposed by Biscaia et al. [63,80,81] is used:

$$\varepsilon_r = \frac{1}{1+\rho}\cdot\frac{ds}{dx} \tag{17}$$

where ρ is the ratio between the axial stiffnesses of the FRP composite and the substrate. Hence, at $x = 0$, the slip is s_0 and introducing Eq. (16) into Eq. (17), the FRP strains at the tip of the mechanical end anchorage are obtained by:

$$\varepsilon_{r0} = \frac{1}{1+\rho}\cdot\sqrt{2\lambda \cdot G_F \cdot \left(1 - e^{-B \cdot s_0}\right)^2 + C_1} \tag{18}$$

Consequently, the value of constant C_1 is

$$C_1 = {\varepsilon_{r0}}^2 \cdot (1+\rho)^2 - D^2 \cdot \left(1 - e^{-B \cdot s_0}\right)^2 \tag{19}$$

where D is a positive constant defined according to

$$D = \sqrt{2\lambda \cdot G_F} \tag{20}$$

Therefore, the FRP strains are defined as

$$\varepsilon_r = \frac{1}{1+\rho}\cdot\sqrt{D^2 \cdot \left(1 - e^{-B \cdot s}\right)^2 + {\varepsilon_{r0}}^2 \cdot (1+r)^2 - D^2 \cdot \left(1 - e^{-B \cdot s_0}\right)^2} \tag{21}$$

It should be noted that since D depends on the parameter λ, in the case of an FRP strip bonded according to the Near Surface Mounted (NSM) technique or the case of an FRP rod, it can be redefined. So, Eq. (3) can be adjusted to the bonding technique, i.e., EBR, NSM or with an FRP rod. Thus, for the NSM technique and for the case of using an FRP rod, Eq. (20) can be redefined, respectively, according to:

$$D = \sqrt{4\frac{G_F}{t_r}\left(\frac{1}{E_r} + \frac{t_r \cdot b_r}{2E_s \cdot t_s \cdot b_s}\right)} \tag{22}$$

and

$$D = \sqrt{8G_F \cdot \left(\frac{1}{E_r \cdot \phi_r} + \frac{\pi \cdot \phi_r}{4E_s \cdot t_s \cdot b_s}\right)} \tag{23}$$

where ϕ_r is the diameter of the FRP rod. Consequently, the analytical derivations carried out from this point forward can also be applied to those two cases by using the correct value of parameter D obtained from Eqs. (20), (22) and (23).

To define the slips developed throughout the FRP-to-substrate interface, Eq. (16) is rewritten according to

$$\frac{ds}{\sqrt{\left(1 - e^{-B \cdot s}\right)^2 + \left(\frac{\sqrt{|C_1|}}{D}\right)^2}} = D dx \tag{24}$$

Integrating Eq. (24) leads to

$$\frac{D \cdot \operatorname{arsinh}\left(\frac{\left(D^2 + C_1\right) \cdot e^{B \cdot s} - D^2}{\sqrt{|C_1|} \cdot D}\right)}{B \cdot \sqrt{|D^2 + C_1|}} = D \cdot x + C_2 \tag{25}$$

where C_2 is a constant that can be defined through the slips developed at the tip of the mechanical anchorage. Thus, as already mentioned, at point $x = 0$, the slips are $s = s_0$, and solving Eq. (25) with respect to s, the slips developed throughout the bonded length of the mechanically anchored joint are defined according to

$$s(x) = \frac{1}{B} \cdot \ln\left[\frac{D^2 + \sqrt{|C_1|} \cdot D \cdot \sinh\left(\frac{B \cdot (D \cdot x + C_2) \cdot \sqrt{|D^2 + C_1|}}{D}\right)}{|D^2 + C_1|}\right] \tag{26}$$

where

$$C_2 = \frac{D \cdot \operatorname{arsinh}\left(\frac{\left(D^2 + C_1\right) \cdot e^{B \cdot s_0} - D^2}{\sqrt{|C_1|} \cdot D}\right)}{B \cdot \sqrt{|D^2 + C_1|}} \tag{27}$$

The FRP strains developed throughout the bonded length are obtained by introducing Eq. (26) in Eq. (21):

$$\varepsilon_r(x) = \frac{1}{1+\rho} \cdot \frac{\sqrt{|C_1 + D^2|} \cdot \cosh\left(\frac{B \cdot (D \cdot x + C_2) \cdot \sqrt{|C_1 + D^2|}}{D}\right)}{\sinh\left(\frac{B \cdot (D \cdot x + C_2) \cdot \sqrt{|C_1 + D^2|}}{D}\right) + \frac{D}{\sqrt{|C_1|}}} \tag{28}$$

For the definition of the shear bond stresses developed throughout the bonded length of the mechanically anchored joint, Eq. (26) is introduced in Eq. (8), leading to

$$\tau_b(x) = B{\cdot}G_F{\cdot}\frac{\frac{D}{\sqrt{|C_1|}}+\frac{\sqrt{|C_1|}}{D}}{\frac{D}{\sqrt{|C_1|}}+\sinh\left(B{\cdot}(D{\cdot}x+C_2){\cdot}\sqrt{\left|1+\frac{C_1}{D^2}\right|}\right)} \times\left(1-\frac{\frac{D}{\sqrt{|C_1|}}+\frac{\sqrt{|C_1|}}{D}}{\frac{D}{\sqrt{|C_1|}}+\sinh\left(B{\cdot}(D{\cdot}x+C_2){\cdot}\sqrt{\left|1+\frac{C_1}{D^2}\right|}\right)}\right) \tag{29}$$

The strains developed in the substrate can also be found by following the expression already derived by Biscaia et al. [63,80,81]:

$$\varepsilon_s = -\frac{1}{1+\frac{1}{\rho}}\cdot\frac{ds}{dx} \tag{30}$$

Then, introducing Eq. (16) in Eq. (30) yields

$$\varepsilon_s(x) = -\frac{1}{1+\frac{1}{\rho}}\cdot\frac{\sqrt{|C_1+D^2|}\cdot\cosh\left(\frac{B{\cdot}(D{\cdot}x+C_2){\cdot}\sqrt{|C_1+D^2|}}{D}\right)}{\sinh\left(\frac{B{\cdot}(D{\cdot}x+C_2){\cdot}\sqrt{|C_1+D^2|}}{D}\right)+\frac{D}{\sqrt{|C_1|}}} \tag{31}$$

It should be noted that Eqs. (26), (28), (29), and (31) all depend on s_0 and ε_{r0}, and for this reason, the relationship between these two parameters should be known to predict the complete debonding process of the FRP-to-substrate joint. In other words, the strain-slip (ε_{r0}-s_0) relationship of the axial spring should be known. Since no particular case is set for the strain-slip relationship, the use of any type of strain-slip (or load-slip) relationship, linear or nonlinear, is allowed in this analytical model.

2.2. Advantages and limitations of the analytical model

The present analytical model has some advantages that are highlighted below. Also, the advantages identified here take into account other existing analytical models, e.g. [54,55,57,82,83]. Thus, it can be observed that the analytical model is relatively simple to use. Since the exponential bond-slip relationship is not a piecewise function, all the states that the FRP-to-substrate with a transversely compressed end mechanical anchorage undergoes until its complete debonding are obtained from a single formula (i.e. Eq. (28)) regardless of the total bonded length of the joint. Considering a long-bonded length and until its complete debonding, the mechanically anchored joint should go through 5 different states, namely, E, E-S, E-S-D, S-D, and D. So, by using Eq. (28), the shear bond stresses developed throughout the FRP-to-substrate interface at any of those 5 states are determined. Otherwise, a different expression would need to be found for each state of the interface. Since the increment is at the mechanical end anchorage tip (at $x = 0$) and not at the FRP-loaded end, the snap-back phenomenon usually observed in sufficiently long bonded lengths can be captured by the analytical model as well. Moreover, in the cases of a nonlinear spring showing a snap-through phenomenon obtained from, e.g., an FRP-to-substrate joint with multiple debonding defects [63,84], the analytical model can also reflect this phenomenon on the debonding process of the mechanically anchored FRP-to-concrete joint.

Using a nonlinear axial spring to simulate the transversely compressed mechanical anchorage can capture a wider range of cases than any other model. For instance, the analytical model can be used in the case of an end anchorage with a linear behaviour, i.e., modelled by a spring with a linear behaviour as documented in the literature [54,85]. Moreover, if the stiffness of this axial spring is set to a very low value, then it will fall into the case of an FRP-to-substrate bonded joint with no mechanical anchorages, which is a very common situation already described in the literature, e.g. [34,36,55,57–59].

Another advantage of the analytical model is its wider applicability to other bonding techniques. Only the expression to define parameter D needs to be adjusted. Thus, for the case of the EBR technique, Eq. (20) should be used, but in the case of the NSM technique, Eq. (22) should be used instead. Moreover, if FRP rods are used rather than FRP strips or sheets, the analytical model can be used by considering Eq. (23). However, the strain-slip behaviour of the mechanical end anchorage should be known regardless of the bonding technique used due to the reasons explained above.

Despite not being studied here, there are no reasons for the analytical model not to be used with glass (G) or basalt (B) FRP composites bonded to concrete, timber, steel or clay brick substrates. However, it should be kept in mind that the bond-slip relationship between both dissimilar materials should be approximated by Eq. (35). Thus, the main limitation of the analytical model lies in the bond-slip relationship itself. So, if an FRP-to-substrate shows a local bond behaviour that cannot fit through the exponential bond-slip relationship defined in Eq. (8), then the analytical model cannot predict the debonding process of the joint accurately. Within this context, here are a few examples. One is the use of a ductile adhesive that leads to a trapezoidal bond-slip relationship with a long plateau at maximum shear bond stress. Another limitation lies in the case of FRP-to-substrate bonded joints subjected to compressive stress. In the former, a similar exponential bond-slip relationship defined in Eq. (8) was already used by Jiang et al. [86] to approximate the bond behaviour of CFRP-to-steel joints with a ductile adhesive, for the latter, the use of the exponential bond-slip relationship in Eq. (8) is out of the question. In this case, the main issue is the friction stress generated at higher slip values due to the external compressive stresses applied to the FRP-to-substrate joint, which is not supported by the exponential bond-slip relationship defined in Eq. (8), in which the shear bond stresses approach zero for higher slip values rather than a residual nonzero value.

A couple of obvious limitations of the analytical model are identified below. Since the analytical model deals only with a monotonic slip increment, the cases where the FRP-to-substrate joints are subjected to cyclic loading cannot be simulated. Regardless of the loading protocol history adopted for the bonded joint, the other limitation lies in those joints where a temperature variation is considered.

3. Validation strategy

To validate the analytical model, a series of different specimens and some experimental results found in the literature are considered. To assess the influence of the anchorage length on the final bond performance of the CFRP-to-substrate joints with a transversely compressed mechanical anchorage, the first case assumed short and long anchorages. At the same time, two different compressive stress magnitudes are also assumed. For simplicity, the friction angle (ϕ) is kept the same in all the specimens. As already explained in Subsection 2.2, the analytical model cannot be used to predict the strain-slip relationship of the mechanical anchorage, and for this reason, two numerical procedures, one based on the Finite Difference Method (FDM) and another one based on the bond-slip relationship discretisation, are developed and used instead. Thus, based on the prediction of the strain-slip (ε_{r0}-s_0) relationship, the analytical model is used to predict the debonding process of the transversely compressed FRP-to-substrate joints and the results are compared to those obtained from the Finite Element Method (FEM). After the validation of the analytical model, its accuracy is analysed using experimental data found in the literature [48–50]. The experimental bond-slip relationships reported in those studies [48–50] are used to obtain the strain-slip curves and then used in the analytical model so that the bond performance of the experiments can be analytically predicted.

3.1. Determining the strain-slip relationship of transversely compressed bonded joints

3.1.1. Numerical model with the Finite Difference Method (FDM)

As already mentioned, to obtain the strain-slip response of the mechanical anchorage and simulate it through an axial spring, the exponential bond-slip relationship defined by Eq. (8) cannot be used since it does not consider any friction branch for higher slip values. So, to bypass this issue, the following bond-slip relationship originally proposed by the authors in another work [87] is considered:

$$\tau_b(s) = \beta \cdot \tau_{b,\,\max} \cdot \left(1 - e^{-b \cdot s}\right) \cdot \frac{\frac{\tau_{b,f}}{\beta \cdot \tau_{b,\,\max}} + e^{-a \cdot (s - s_t)}}{1 + e^{-a \cdot (s - s_t)}} \tag{32}$$

where β is a dimensionless parameter that ensures the maximum shear bond stress is reached and can be obtained by a simple trial and error process; a and b are two parameters to be calibrated with the experimental data; and s_t is the slip that usually corresponds to the midpoint of the transition between the maximum ($\tau_{b,\max}$) and the frictional ($\tau_{b,f}$) stresses. Since the influence of the compressive stresses on the shear bond stresses can be described by the Mohr-Coulomb failure criterion, e.g. [45,46,84], $\tau_{b,\max}$ and $\tau_{b,f}$ can be determined, respectively, according to:

$$\tau_{b,\,\max} = \tau_{b,\,\max\,0} + \tan(\phi) \cdot \sigma_n \tag{33}$$

and

$$\tau_{b,f} = \tan(\phi) \cdot \sigma_n \tag{34}$$

where σ_n is the compressive stress applied to the FRP-to-substrate interface with a positive signal. Introducing Eq. (33) and Eq. (34) in Eq. (32) yields:

$$\tau_b(s) = \beta \cdot \left(\sigma_n \cdot \tan(\phi) + \tau_{b,\,\max\,0}\right) \cdot \left(1 - e^{-b \cdot s}\right) \cdot \frac{\frac{\sigma_n \cdot \tan(\phi)}{\beta \cdot \left(\sigma_n \cdot \tan(\phi) + \tau_{b,\,\max\,0}\right)} + e^{-a \cdot (s - s_t)}}{1 + e^{-a \cdot (s - s_t)}} \tag{35}$$

Fig. 3 shows the main differences between the bond-slip relationship defined in Eq. (35) with Eq. (8), i.e., between Biscaia and Carmo's proposal [87] and Dai's et al. [47] proposal, respectively. It should also be noted that Biscaia and Carmo's proposal [87] can be used for FRP-to-substrate joints with or without a transversely compressed anchorage. In this case, the frictional stress parameter should be considered zero, which, like Dai's et al. [47] proposal, makes the shear bond stresses tend to a zero value with the slip increase.

The governing equation of the debonding process of the FRP-to-concrete joints subjected to compressive stresses is obtained by introducing Eq. (35) in Eq. (2), i.e.:

$$\frac{d^2 s}{dx^2} - \lambda \cdot \beta \cdot \left(\sigma_n \cdot \tan(\phi) + \tau_{b,\,\max\,0}\right) \cdot \left(1 - e^{-b \cdot s}\right) \cdot \frac{\frac{\sigma_n \cdot \tan(\phi)}{\beta \cdot \left(\sigma_n \cdot \tan(\phi) + \tau_{b,\,\max\,0}\right)} + e^{-a \cdot (s - s_t)}}{1 + e^{-a \cdot (s - s_t)}} = 0 \tag{36}$$

The analytical solution of Eq. (36) is not known, and for this reason, the FDM is applied to solve it. To that end, the bonded joint is discretised first into equidistant n points, and a regular step is defined as

$$h = \frac{L_a}{n} \tag{37}$$

where L_a is the anchorage length of the joint as shown in Fig. 2. Then, the following approximations are used:

$$\frac{ds(x_i)}{dx} \approx \frac{s_{i+1} - s_{i-1}}{2h} \text{ with } i = 0, 1, 2, \ldots, n \tag{38}$$

and

$$\frac{d^2 s(x_i)}{dx^2} \approx \frac{s_{i+1} - 2s_i + s_{i-1}}{h^2} \text{ with } i = 0, 1, 2, \ldots, n \tag{39}$$

Then, the Newton-Raphson iterative technique is used to obtain the solution of the generated system of nonlinear equations, i.e.:

$$\{s_i\}_{j+1} = \{s_i\}_j - [J(s_i)]^{-1} \cdot \{f_i(s_i)\} \tag{40}$$

where the column vector $\{f_i(s_i)\}$ corresponds to the first member of Eq. (35) at point i; $\{s_i\}_{j+1}$ and $\{s_i\}_j$ are, respectively, the column vectors of the slips at each discretised point of the anchored length in the $j+1$-th and j-th iterations; and $[J(s_i)]^{-1}$ is the inverse of the Jacobian matrix defined by:

$$[J(s_i)] = \begin{bmatrix} \frac{\partial f_0(s_0, s_1)}{\partial s_0} & \frac{\partial f_0(s_0, s_1)}{\partial s_1} & \frac{\partial f_0(s_0, s_1)}{\partial s_2} & \cdots & \frac{\partial f_0(s_0, s_1)}{\partial s_{n-1}} \\ \frac{\partial f_1(s_0, s_1, s_2)}{\partial s_0} & \frac{\partial f_1(s_0, s_1, s_2)}{\partial s_1} & \frac{\partial f_1(s_0, s_1, s_2)}{\partial s_2} & \cdots & \frac{\partial f_1(s_0, s_1, s_2)}{\partial s_{n-1}} \\ \frac{\partial f_2(s_1, s_2, s_3)}{\partial s_0} & \frac{\partial f_2(s_1, s_2, s_3)}{\partial s_1} & \frac{\partial f_2(s_1, s_2, s_3)}{\partial s_2} & \cdots & \frac{\partial f_2(s_1, s_2, s_3)}{\partial s_{n-1}} \\ \vdots & \vdots & \vdots & \ddots & \vdots \\ \frac{\partial f_{n-1}(s_{n-2}, s_{n-1})}{\partial s_0} & \frac{\partial f_{n-1}(s_{n-2}, s_{n-1})}{\partial s_1} & \frac{\partial f_{n-1}(s_{n-2}, s_{n-1})}{\partial s_2} & \cdots & \frac{\partial f_{n-1}(s_{n-2}, s_{n-1})}{\partial s_{n-1}} \end{bmatrix}. \tag{41}$$

The debonding processes of the FRP-to-substrate bonded joints subjected to compressive stress can be simulated by a displacement control at the front tip of the end anchorage, i.e., at $x = n$, or the back of the end anchorage, i.e., at $x = 0$, of the discretised anchored length. The choice of which displacement control point should be used will depend on the need to capture the snap-back phenomenon of the FRP-to-substrate bonded joint. Nevertheless, it should be noted that the snap-back phenomenon is only obtained if the anchorage length is sufficiently long. Since the slips at the front tip of the anchorage are not monotonic until failure, the snap-back phenomenon is obtained if the control displacement is set at the back of the end anchorage, where the slips at $x = 0$ are always monotonic until failure. In this latter case, Eq. (41) should be adjusted to the boundary condition of the slip control increment at the back of the anchorage, and the FRP strain at $x = n$ should be determined from Eq. (17). Regardless of the displacement control considered, the FRP strains developed at the back of the end anchorage are always zero during the complete debonding process of the

joint. Thus, the second boundary condition is $ds(x)/dx = 0$, which, considering Eq. (38), leads to $s_1 = s_{-1}$. The final solution of a given slip increment is found when the column vector of the slips at iteration $j+1$ is similar to the previous column vector of the slip at iteration j, i.e., when:

$$\{s_i\}_{j+1} - \{s_i\}_j \approx 0 \tag{42}$$

which is usually reached for a low number of iterations, but, in the present case, it was limited to a maximum of 500 possible iterations to solve Eq. (40).

3.1.2. Numerical procedure based on the bond-slip relationship

As an alternative to the numerical procedure described in the previous subsection, another numerical procedure can be used, which, to the authors' best knowledge, is introduced here for the first time. Although it is much easier than the previous one, this procedure has some limitations that will be pointed out in this subsection. Thus, let us first assume that the strain-slip relationship is known, but the local bond behaviour of the bonded joint is not. In that case, and if the known strain-slip relationship is from a bonded joint with a sufficiently long bond length, then Eq. (5) can be used to obtain the bond-slip relationship. To that end, the shear bond stress at a given slip can be obtained by combining Eq. (5) and Eq. (17) in its approximate form, i.e.:

$$\tau_{b,i+1} = E_r \cdot t_r \cdot (1+\rho) \cdot \frac{\varepsilon_{r,i+1} - \varepsilon_{r,i}}{s_{i+1} - s_i} \cdot \varepsilon_{r,i+1} \tag{43}$$

where $\tau_{b,i+1}$ is the shear bond stress at point $i+1$ of the strain-slip relationship; $\varepsilon_{r,i+1}$ and $\varepsilon_{r,i}$ are the FRP strains at point $i+1$ and i of the strain-slip relationship, respectively; and s_{i+1} and s_i are the slips at point $i+1$ and i of the strain-slip relationship, respectively.

If the bond-slip relationship of the bonded joint is known but the strain-slip relationship is not, then Eq. (43) can be solved by isolating ε_{i+1}, which leads to:

$$\varepsilon_{r,i+1}{}^2 - \varepsilon_{r,i} \cdot \varepsilon_{r,i+1} - \frac{\tau_{b,i+1} \cdot (s_{i+1} - s_i)}{E_r \cdot t_r \cdot (1+\rho)} = 0 \tag{44}$$

The solution of the 2nd-order polynomial equation stated in (44) allows us to determine the FRP strains at s_{i+1}, i.e.:

$$\varepsilon_{r,i+1} = \frac{\varepsilon_{r,i}}{2} + \sqrt{\left(\frac{\varepsilon_{r,i}}{2}\right)^2 + \frac{\tau_{b,i+1} \cdot (s_{i+1} - s_i)}{E_r \cdot t_r \cdot (1+\rho)}} \tag{45}$$

Hence, the strain-slip relationship to be used with the analytical model can be experimentally obtained, or it can be derived from Eq. (45) and using Eq. (32) regardless of the compressive stress magnitude of the bonded joint. By using Eq. (45), the snap-back phenomenon cannot be captured, which, admittedly only in the final section, compromises the correct definition of the complete debonding process of the FRP-to-substrate joints with a transversely compressed mechanically end anchorage. However, since the snap-back is a theoretical concept only, this numerical procedure can be used on experimental data.

It should also be kept in mind that the prediction of the strain-slip relationship from the bond-slip relationship should be carried out only for sufficiently long bonded joints, which, in the present work, limits the analysis to long anchorages. On the other hand, however, if the bonded anchorage is too short, then uniform shear bond stresses can be considered throughout the anchorage length, and so the strain-slip relationship can be obtained by multiplying the shear bond stress in the end anchorage area, which avoids the use of Eq. (45).

3.2. Description of the generated cases

This subsection presents a comprehensive description of all generated cases, namely, materials, dimensions and geometries. So, the identification of each generated specimen is also presented. Thus, the

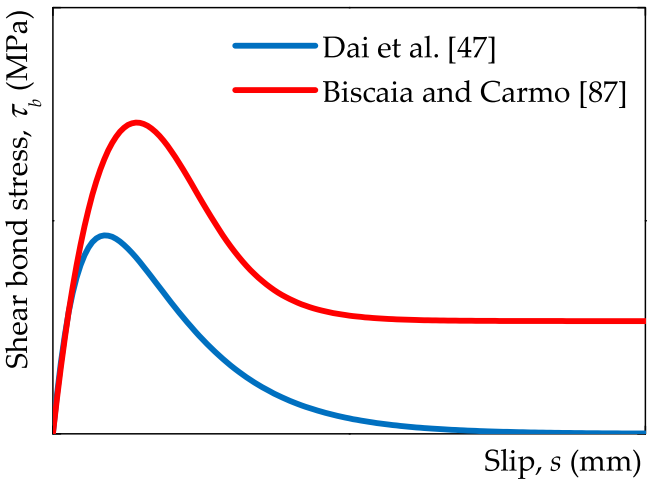

Fig. 3. Comparison between the exponential bond-slip relationship proposed by Dai et al. [47] and that proposed by Biscaia and Carmo [87].

specimens to be tested under the pull-push test consist of a unidirectional CFRP composite externally bonded to a concrete block by an epoxy resin with a brittle constitutive behaviour such as S&P Resin 220HP [88], which, according to the datasheet of the manufacturer, has an elastic modulus of 7.1 GPa and a tensile strength of 15 MPa.

The materials used were based on the work carried out by Aghabagloo et al. [89], in which the CFRP strip was 50 mm wide and 1.4 mm thick, whilst the concrete block measured 200 × 200 × 400 mm (width × thickness × length). According to the datasheet of the manufacturer [90], the mechanical properties of the CFRP strip were as follows: elastic modulus of 170 GPa, ultimate tensile strength of 2800 MPa and a rupture strain of 1.64 %. The mechanical properties of the concrete were obtained from the test of concrete cylinders measuring 150 × 300 mm (diameter × length), which led to a mean compressive strength of 41.6 MPa and an elastic modulus of 33.9 GPa.

The bond-slip relationships obtained by Aghabagloo et al. [89] were derived from a teaching-learning-based optimisation (TLBO) algorithm, which, in the case of the EBR system free of any mechanical anchorage, led to a maximum shear bond stress of 9.3 MPa with a corresponding slip of 0.031 mm, with a pure Mode-II fracture energy of approximately 0.713 N/mm. These values were used to obtain an equivalent bond-slip relationship by using Eq. (8). To that end, the least square minimisation between the bond-slip relationship obtained by Aghabagloo et al. [89] and that obtained from Eq. (8) was carried out, adopting the fracture energy and the maximum shear bond stress as constraints in the minimisation process, i.e., ensuring that the same maximum shear stress and fracture energy were obtained. Then, the stiffness index of the CFRP-to-concrete bonded joint was determined, i.e. $B = 26.13\ \text{mm}^{-1}$. For the bond-slip relationship of the CFRP-to-concrete joints with a transversely compressed end anchorage, the maximum shear bond stress obtained by Aghabagloo et al. [89] was 11.4 MPa with a corresponding slip of 0.030 mm and a frictional stress of approximately 5.3 MPa. As well as bonding the CFRP composite to the concrete substrate, Aghabagloo et al. [89] also bonded the anchorage to the CFRP composite. Consequently, this CFRP-to-concrete joint did not follow the Mohr-Coulomb rupture criterion as it was expected to. So, to preserve the condition stated in Eq. (33), the maximum shear bond stress is $\tau_{b,\max} = 14.6$ MPa. Given the lack of further data to calculate the friction angle of the CFRP-to-concrete joint, it was assumed $\phi = 1.0$ rad, which is a reasonable value considering several tests performed by Biscaia et al. [91–93] on GFRP-to-concrete bonded joints. Thus, the calculated compressive stress is approximately $\sigma_n = 3.4$ MPa. When adjusted to the bond-slip relationship reported by Aghabagloo et al. [89] through the same least square minimisation process mentioned earlier, the bond-slip relationship defined in Eq. (35) led to the following parameters: a

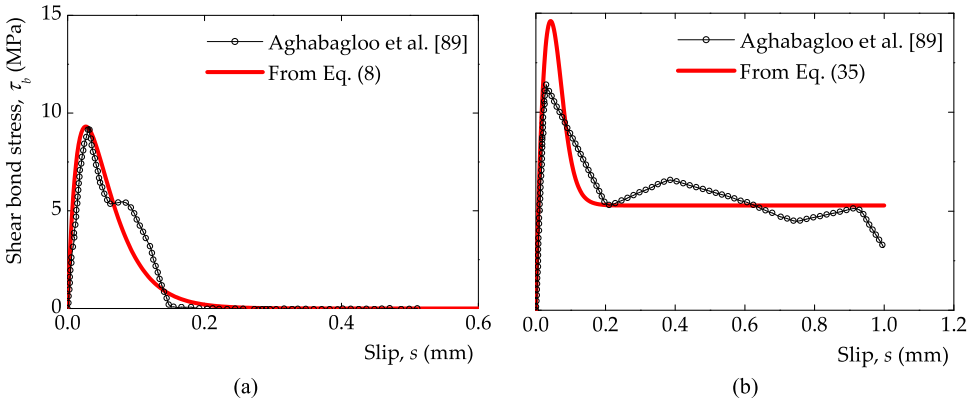

Fig. 4. Bond-slip relationships obtained for the CFRP-to-concrete bonded joints tested by Aghabagloo et al. [89]: (a) free of any mechanical anchorages; and (b) with a transversely compressed mechanical end anchorage.

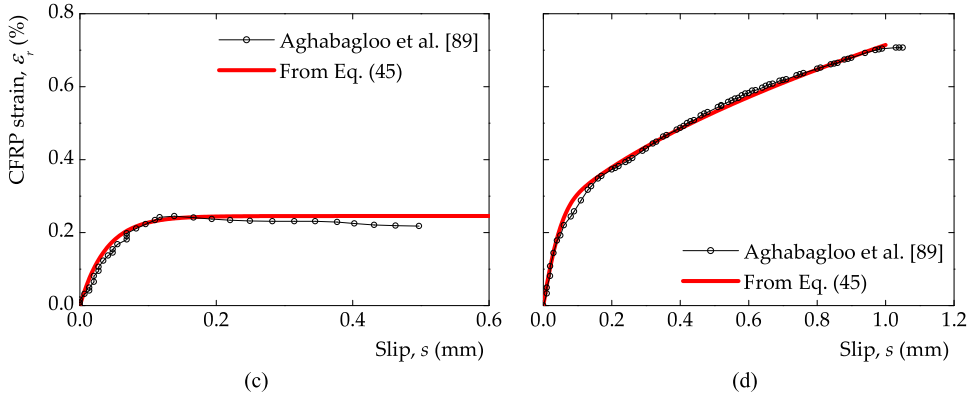

Fig. 5. Strain-slip relationships obtained for the CFRP-to-concrete bonded joints tested by Aghabagloo et al. [89] using the proposed numerical procedure in Eq. (45): (a) free of any mechanical anchorages; and (b) with a transversely compressed mechanical end anchorage.

$= 47.149$, $b = 36.532$, $s_t = 0.061$ mm, $\beta = 1.641$, and $\tau_{b,f} = 5.3$ MPa. Fig. 4a and Fig. 4b compare the experimental bond-slip relationships obtained by Aghabagloo et al. [89] and those obtained by Eq. (8) and Eq. (35), respectively. Based on these results, Eq. (45) was used to predict the strain-slip relationship of the CFRP-to-concrete bonded joints. Figs. 5a and 5b compare the strain-slip relationships obtained from the experiments carried out by Aghabagloo et al. [89] and those predicted by Eq. (45).

Based on these results, a series of specimens was idealised, and their bond performance was studied thoroughly. For simplicity and to avoid unnecessarily increasing the size of the text, two anchorages (L_a) and bonded lengths (L_b) of 50 mm and 260 mm are considered, as well as two different external compressive stresses (σ_n) of 1.7 MPa and 3.4 MPa. In addition, two other specimens were idealised where the load needed to be applied to the 50 mm long anchorage and develop a compressive stress of 3.4 MPa on the 260 mm long anchorage (44.20 kN). As a result, the transversely compressed mechanical end 50mm-long anchorage will be subjected to a compressive stress of 17.68 MPa. In this idealised case, the maximum shear bond stress and the friction stress of the bond-slip relationship defined in Eq. (35) are, respectively, $\tau_{b,\max} = 36.85$ MPa and $\tau_{b,f} = 27.53$ MPa and with $\beta = 1.451$ (other parameters were unchanged). These stress values are too high and, in practice, may easily lead to the rupture of the CFRP carbon fibres during the application of the loads on the mechanical anchorage, which will ruin the CFRP-to-concrete joint. Despite this, such a scenario was considered so that the influence of the same load applied to the anchorage could be analysed, regardless of its length.

The case with no external compressive stress is also considered in order to obtain reference data. A total of twenty-five specimens were

Table 1
ID of the generated specimens.

ID	Compressive stress (σ_n)	Anchorage length, L_a (mm)	Bonded length, L_b (mm)	Total length, L_t (mm)
CC0–0–50	0	0	50	50
CC0–0–100	0	0	100	100
CC0–0–260	0	0	260	260
CC0–0–310	0	0	310	310
CC0–0–520	0	0	520	520
CC1.7–50–0	1.7	50	0	50
CC1.7–100–0	1.7	100	0	100
CC1.7–260–0	1.7	260	0	260
CC1.7–310–0	1.7	310	0	310
CC1.7–520–0	1.7	520	0	520
CC3.4–50–0	3.4	50	0	50
CC3.4–100–0	3.4	100	0	100
CC3.4–260–0	3.4	260	0	260
CC3.4–310–0	3.4	310	0	310
CC3.4–520–0	3.4	520	0	520
CC1.7–50–50	1.7	50	50	100
CC1.7–50–260	1.7	50	260	310
CC1.7–260–50	1.7	260	50	310
CC1.7–260–260	1.7	260	260	520
CC3.4–50–50	3.4	50	50	100
CC3.4–50–260	3.4	50	260	310
CC3.4–260–50	3.4	260	50	310
CC3.4–260–260	3.4	260	260	520
CC17.68–50–50	17.68	50	50	100
CC17.68–50–260	17.68	50	260	310

considered, whose designation begins with the materials used and external compressive stress, followed by the anchorage and bonded length, respectively. For instance, specimen CC3.4–50–260 means that a CFRP composite is externally bonded to a concrete substrate with an end anchorage of 50 mm, subjected to an external compressive stress of 3.4 MPa and has a bonded length of 260 mm. Table 1 summarises the ID of the generated specimens under study in this work.

3.3. Finite Element Method (FEM)

The FEM is used to validate the analytical model. Different commercial software programs have been used in the literature to model the bond behaviour between an FRP composite bonded to a substrate, e.g. [52,53,94–97]. Among these, the commercial software ATENA [98] was selected, which has already been used with success to model several debonding processes of FRP-to-substrate bonded joints subjected to different conditions, e.g. [45,46,80,99]. To significantly reduce both the number of unknowns and nonlinear equations to be solved by the Newton-Raphson method and the time required to process the numerical simulations, the 2D version of the FEM was used. What is more, the 2D version of the FEM is as close to the key assumptions of the analytical model as possible, allowing fair comparisons to be made between them.

The dimensions and geometries of the models were the same as the studied specimens. The concrete block was modelled by the "SBETA Material", which is a material available in the ATENA [98] material library, whereas the CFRP composite was modelled with the "Plane Strain Elastic Isotropic" material. The mechanical properties used to define the CFRP and the concrete block were the same as those earlier reported in Subsection 3.2. The contact between the CFRP and the concrete was modelled through a coupled cohesive zone model (CZM) based on the Mohr-Coulomb rupture criterion with tension cut-off, which is denoted as "2D Interface" material in ATENA's library [98]. The CZM considers the influence of the peeling stresses (normal bond stresses developed perpendicularly to the shear bond stresses, i.e. in the direction coincident with fracture Mode I), on the shear bond stresses through the Mohr-Coulomb failure criterion. Therefore, the friction angle (ϕ) of the CFRP-to-concrete interface should be defined correctly because it has a significant impact on the bond performance in the debonding process of transversely compressed mechanical joints due to the presence of a mixed mode (mode I+II) condition [45,46,84].

The loads applied to the CFRP strip (no. 4 in Fig. 6) were simulated by a regular monotonic displacement of 0.002 mm per step that was applied to the right-hand side of the CFRP end (see no. 7 in Fig. 6). The simulations were all controlled by three monitoring points (see no. 9 in Fig. 6). The first monitoring point was placed at the same point where the monotonic displacements were imposed on the model. The other two monitoring points controlled the loads transmitted to the CFRP composite and to the nonlinear spring (see no. 6 in Fig. 6). The concrete block (see no. 1 in Fig. 6) was supported by a series of pinned roller supports (see no. 2 in Fig. 6), and a reaction steel plate (no. 3 in Fig. 6) was placed at the righthand of the specimen, where a pinned roller support was placed at its midpoint. It should be noted that the model has two reaction steel plates, one in front of the concrete block and the other in front of the CFRP composite, ensuring that the displacements were all the same in all the nodes of the CFRP-loaded end. However, between these two steel plates, no contact between them was considered (see no. 5 in Fig. 6). Unlike this contactless region, the contact between the CFRP and the concrete block was ensured by non-thickness contact elements throughout the bonded length of the CFRP-to-concrete joint (see no. 8 in Fig. 6). At the rear of the model, i.e. at the left-hand, a steel plate ensures that all the nodes of the CFRP-unloaded end have the same displacements that are transmitted to the axial spring. Also, between these steel elements and the concrete block, no contact between them is considered.

The end of each incremental step occurred when one of the following convergence criteria was exceeded: displacement error tolerance of 0.01, residual error tolerance of 0.01, absolute residual error tolerance of 0.01, and energy error tolerance of 0.0001. A maximum of 40 iterations was considered in each step, which was sufficient to obtain the numerical results without affecting the accuracy of the simulations. A series of incremental steps was applied to the model so that the complete debonding process of each specimen could be simulated.

The concrete block and the CFRP composite were discretised with a mesh of 5.0 mm of quadrilateral finite elements with smooth shapes. However, near the contacts between the CFRP and the concrete block or between the concrete block and the reaction steel plate, more refined meshes with 0.5 mm and 1.0 mm of the same finite elements were used, respectively. The total number of finite elements used in each specimen varied due to their different bonded lengths. So, from the shortest specimen shown in Fig. 6a (e.g., CC0–0–50, CC3.4–50–0, CC3.4–50–50) to the longest shown in Fig. 6b (CC0–0–520 and CC0–520–0), the number of finite elements used was 1973 and 9703, respectively. In an 11th Gen Intel(R) Core(TM) i9–11900F desktop computer at 2.50 GHz with 32 GB of 2666 MT/s RAM, the simulations were carried out for approximately 5 min to 50 min in the shortest and longest specimens with a transversely compressed anchorage with the same length of the CFRP-to-concrete joint (i.e., specimen CC0–520–0), respectively.

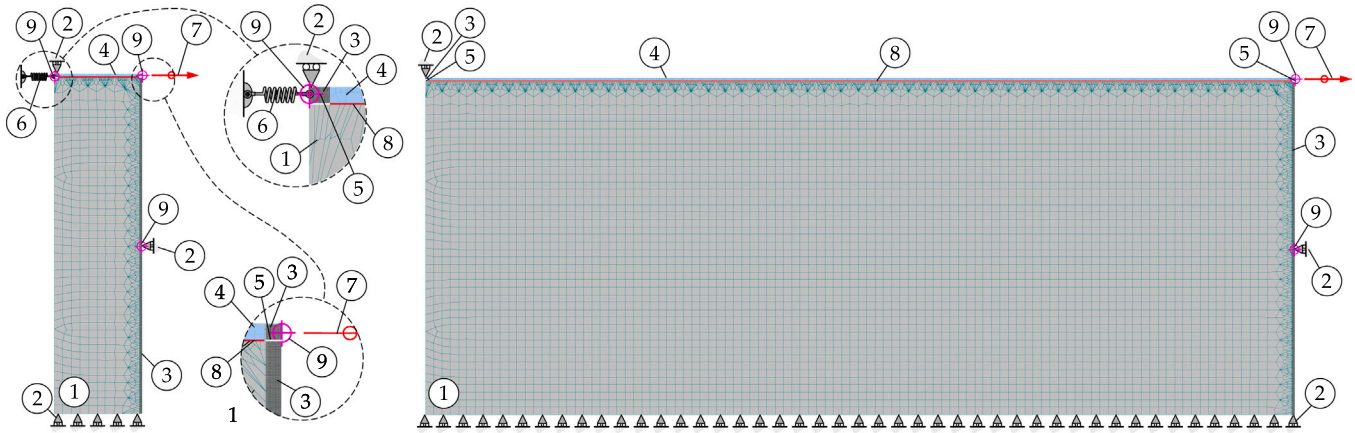

Key: 1 – Concrete substrate; 2 – Roller support; 3 – Rigid material; 4 – CFRP composite; 5 – Interface with no contact; 6 – End anchorage (spring with nonlinear behaviour); 7 – Displacement control; 8 – Interface element; 9 – Load/reaction monitoring point.

Fig. 6. Mesh examples of the transversely compressed mechanical end anchorage of the CFRP-to-concrete joints modelled with the FEM with the: (a) shortest total bonded length, i.e., 50 mm long; and (b) longest total bonded length, i.e., 520 mm long.

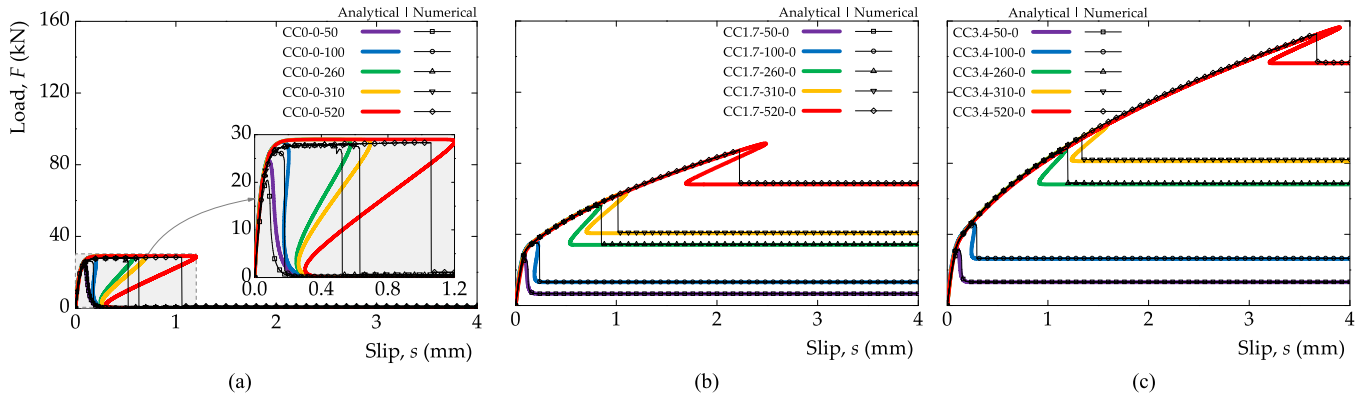

Fig. 7. Load-slip curves obtained from the analytical model and the FEM: (a) specimens with $L_a = 0$; (b) specimens completely compressed with 1.7 MPa; and (c) completely compressed with 3.4 MPa.

4. Discussion of the results

4.1. Load-slip curves

Fig. 7 shows the load-slip curves of all reference specimens. These load-slip curves show the influence of the transversely compressed mechanical anchorage on the CFRP-to-concrete joints when a short and a long anchorage are used. For reference purposes, the load-slip curves shown in Fig. 6a correspond to those cases where the CFRP-to-concrete joints are free of any mechanical anchorage, whereas, in Figs. 6b and 6c, the results obtained from the specimens completely anchored with a compressive stress of 1.7 MPa and 3.4 MPa are considered, respectively. The results shown in Fig. 6a are, as expected, in agreement with similar results documented in the literature, e.g., [34–36,47,64,68,70,94], i.e., as the bonded length increases, the load transmitted to the CFRP-to-concrete joint increases. At a certain bonded length, the maximum loads stopped increasing, and a plateau at maximum load can be seen, which allows us to define the effective bond length of the CFRP-to-concrete joint. Moreover, for the specimens with a bonded length longer than the effective bond length, a snap-back can be seen

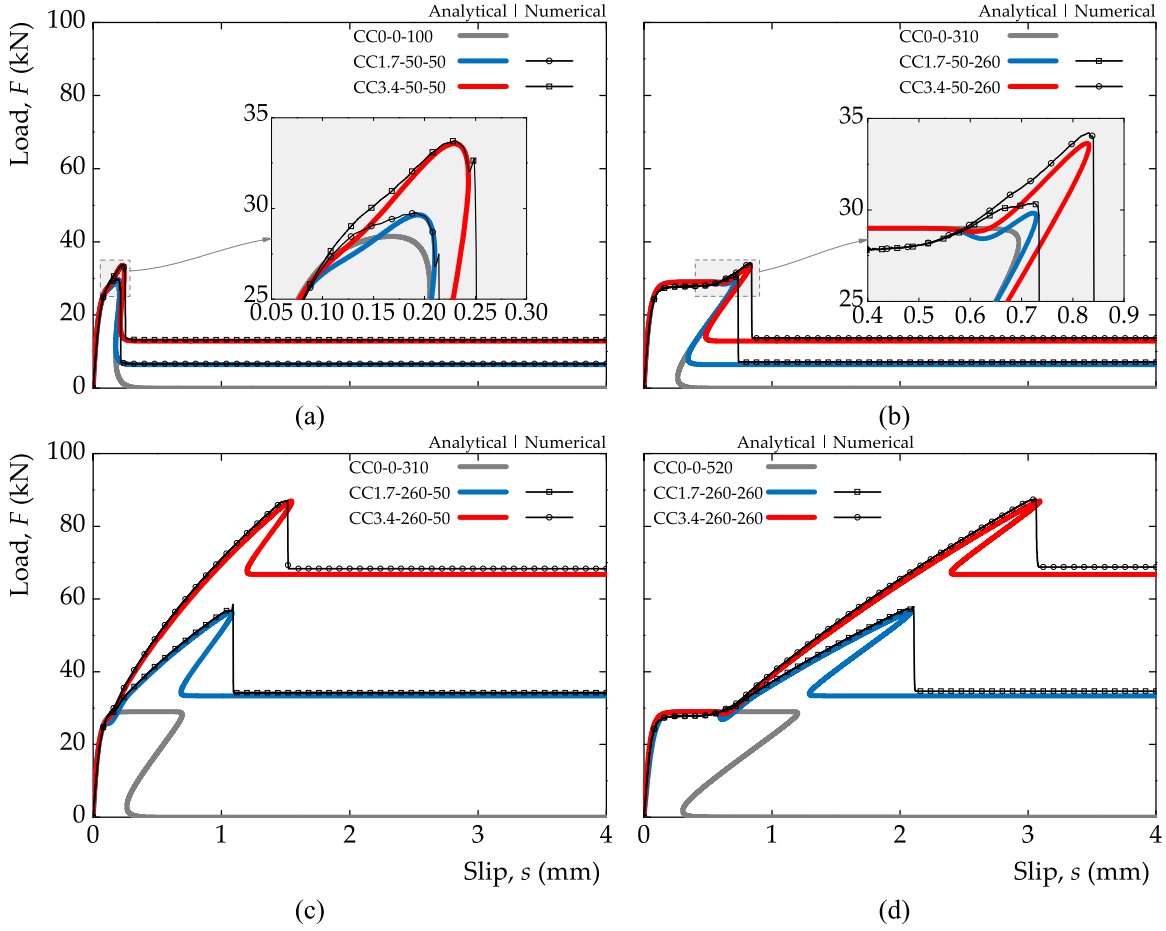

Fig. 8. Load-slip curves obtained from the analytical model and the FEM of the specimens with a transversely compressed anchorage: (a) results from the shortest anchorage and with a total length of 100 mm; (b) results from the shortest anchorage and with a total length of 310 mm; (c) results from the longest anchorage and with a total length of 310 mm; and (d) results from the longest anchorage and with a total length of 520 mm.

before the loads tend to zero with the slip increase.

Comparing the results shown in Figs. 7b and 7c with those shown in Fig. 7a, it can be stated that the load transmitted to CFRP-to-concrete bonded joints increases. This load improvement is more pronounced as the transversal compressive stress increases. As in the longest specimens shown in Fig. 7a, the snap-back phenomenon can be seen in the specimens with the longest anchorage lengths. However, in these cases, the loads transmitted to the CFRP composite do not tend to zero, as do the specimens with longer bonded lengths in Fig. 7a, but rather they tend to a value that corresponds to the friction developed between the CFRP composite and the concrete block instead. In all these reference situations shown in Fig. 7, the analytical results are in good agreement with those obtained from the numerical simulations. However, the maximum loads in the specimens with an anchorage length of 310 mm and 520 mm predicted by the analytical model were overestimated. Thus, in the case of specimens CC1.7–310–0 and CC3.4–310–0, deviations of approximately 2.7 % and 6.8 % were obtained, respectively, whilst deviations of approximately 4.1 % and 2.3 % were found in specimens CC1.7–520–0 and CC3.4–520–0, respectively.

In Fig. 8, the load-slip curves obtained from the CFRP-to-concrete joints with a transversely compressed end anchorage are shown. Figs. 8a and 8b show the influence of using a short transversely compressed end anchorage on the debonding process of the CFRP-to-concrete joints, whilst Figs. 8c and 8d show the influence of using a long end anchorage. Based on these results, it can be stated that the maximum efficiency of using a mechanical end anchorage is achieved only when a long-end anchorage is used rather than when a short anchorage is used, regardless of the magnitude of the transversal compressive stress applied to the end anchorage. Thus, for the 50 mm long end anchorage, the loads transmitted to the CFRP barely improve the final strength of the bonded joints. Although the maximum loads transmitted to the CFRP composite are approximately the same in the specimens with a long-end anchorage, the ductility of the specimens with an additional bonded length of 250 mm is considerably higher. It should also be noted that despite the load capacity improvement obtained from using a transversely compressed end anchorage, the CFRP rupture was never reached in the present situation, which corresponds to 195.16 kN. Thus, to reach such a load magnitude, the compressive stress applied to the anchorage should be greater than 3.4 MPa.

Nevertheless, the compressive stress was increased to 17.68 MPa in the 50 mm long end anchorage, so the same compression load applied on the end anchorage to get a compressive stress of 3.4 MPa could be reached, and so enable us to compare the efficiency of using a short end anchorage with a long one. Fig. 9 shows the load-slip curves of these CFRP-to-concrete joints with a 50 mm long end anchorage. The results show that the maximum load is approximately 80.1 kN in all three specimens, regardless of the additional bonded length of the CFRP-to-concrete joint. Thus, when compared with the specimens with a 260 mm long end anchorage (see Figs. 8c and 8d), the maximum load reached in specimens CC17.8–50–0, CC17.8–50–50 or CC17.68–50–260 is about 8.5 % lower than that reached in specimens CC3.4–260–50 or CC3.4–260–260, which reached approximately 86.9 kN in both specimens. The same occurs with the ductility of the specimens, i.e., lower ductility is obtained in the specimens with a compressive stress of 17.8 MPa. Despite some differences observed on the load-slip curves of specimen CC17.68–50–0, the results obtained from the analytical model are very close to the numerical simulations. Finally, it should be kept in mind, as mentioned earlier, that by increasing the transversal compressive stress of the end anchorage too much, the shear rupture of a significant amount of the CFRP carbon fibres could occur, which damages the integrity of the CFRP composite, consequently, permanently damaging the CFRP-to-concrete bonded joint.

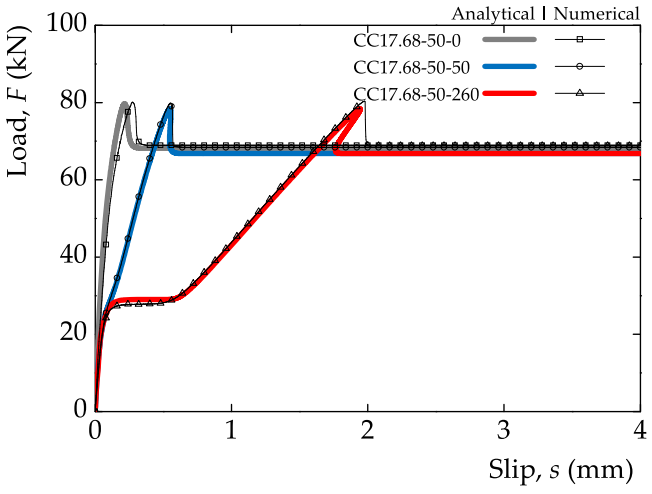

Fig. 9. Load-slip curves obtained from the analytical model and the FEM of the specimens with the same compression load and a 50 mm long end anchorage.

5. Comparisons with other studies

To check the versatility and wide application of the analytical model, three experimental studies found in the literature [48,49] are considered in this section. These three studies are dedicated to the bond behaviour of FRP-to-concrete joints with a transversely compressed mechanical end-anchorage. A brief description of the experimental work and data needed to carry out the analytical simulations can be found in the next subsections. Nevertheless, the reader is advised to consult the sources for deeper insights into these three studies.

5.1. Tests carried out by Barris et al. [48]

Barris et al. [48] conducted a series of tests on CFRP-to-concrete bonded joints with a transversely compressed mechanical end anchorage. The mechanical anchorage is commercially sold by S&P Company, and it was used to anchor CFRP strips 50 mm, 80 mm and 100 mm wide and 1.2 mm thick. The CFRP strips were externally bonded with two-component epoxy S&P resin 220 to a C30/37 concrete block with 200 × 500 × 800 mm (thickness × width × length). The specimens were tested under the pull-push test condition until their rupture. The mechanical properties of the three CFRP strips were obtained from the test of six specimens, and their mean results are summarised in Table 2. From the test of six concrete cylinders measuring 150 × 300 mm (diameter × height), the mechanical properties of the concrete blocks are as follows: elastic modulus of 24.7 GPa and a compressive strength of 33.3 MPa.

The transversely compressed mechanical end anchorage of the CFRP-to-concrete bonded joints consisted of an end anchorage measuring 12 × 200 × 272 mm (thickness × width × length), made of hard aluminium. It has six holes with 18 mm in diameter that are meant to accommodate M16 bolts. Barris et al. [48] used six M16 grade 8.8 steel bolts and considered different torque magnitudes, 0 N·m, 100 N·m and 150 N·m. With a shorter set of specimens, the authors [48] also considered a higher torque magnitude of 200 N·m and, in this case, six M16 grade 10.9 steel bolts were used.

The authors [48] reported the load-slip curves of the tests, and they

Table 2
Mechanical properties of the CFRP strips used in the study carried out by Barris et al. [48].

CFRP strip	Width (mm)	Elastic modulus (GPa)	Tensile strength (MPa)	Rupture strain (%)
L50	50	176.4	2222.4	1.25
L80	80	170.5	2428.0	1.46
L100	100	169.4	2480.2	1.46

Table 3
Parameters for the definition of the exponential bond-slip relationships of the tests carried out by Barris et al. [48].

Original ID of the specimens	Stiffness index (mm^{-1})	Maximum bond stress (MPa)	Maximum slip (mm)	Fracture energy (N/mm)
L50_T30|100|150|200	14.738	4.79	0.047	0.650
L80_T30|100|150|200	13.535	4.15	0.051	0.613
L100_T30|100|150	11.902	3.53	0.058	0.593

also derived the bond-slip relationships obtained from each specimen. The experimental bond-slip relationships were adjusted to the Popovics' formula [100] and, therefore, to use the analytical model defined in Eq. (8), the least square minimisation process between both bond-slip relationships was performed with the maximum shear stress and fracture energy as constraints. The average values of the parameters needed to define the exponential bond-slip relationship in Eq. (8) are summarised in Table 3. The bond-slip relationship defined in Eq. (35) was also approximated so that the local bond behaviour of the transversely compressed end anchorage of the CFRP-to-concrete joints could be simulated. Thus, using a similar minimisation process, all the parameters in Eq. (32) were obtained, and their values are summarised in Table 4.

Fig. 10 compares the load-slip curves obtained from the analytical model with those obtained from the tests carried out by Barris et al. [48]. The analytical results agree with the experimental ones. A first branch is seen in all curves, which corresponds to the debonding process of the CFRP-to-concrete joints limited to the bonded length, i.e., without the influence of the transversely compressed end anchorage. Once the anchorage is activated, the loads transmitted to the CFRP composite tend to increase in a nonlinear way due to the slip of the CFRP composite beneath the anchorage. The analytical model was limited to the strain rupture of the CFRP (see Table 2), which was reached in all three cases. It should be noted that Biscaia and Dai [85] have modelled these same specimens in a previous study, where the mechanical anchorage was modelled with a linear spring. In that case [85], a linear behaviour of the load-slip curves due to the influence of the anchorage on the debonding process of the CFRP-to-concrete joints was obtained, which is not a realistic situation. As can be seen from Fig. 10, the load-slip curves now obtained are closer to the experiments than those obtained by Biscaia and Dai [85], which shows how much more adequate and realistic the present analytical model is to completely simulate the CFRP-to-concrete joints with a transversely compressed mechanical end anchorage. To quantify this superiority of using the nonlinear spring, the Integral Absolute Error (IAE) was used. The IAE is known to be a parameter which is sensitive to the deviation of a theoretical from an experimental result and is often used for model assessment, e.g., [84,85,101,102], and it can be defined as follows:

$$IAE = \sum_{s=1}^{n} \frac{\left|d_{s,AM} - d_{s,Exp}\right|}{\sum_{s=1}^{n} d_{s,Exp}} \tag{46}$$

where $d_{s,AM}$ and $d_{s,Exp}$ correspond to the data obtained from the proposed analytical approach and those experimentally obtained by Barris et al. [48], respectively; and n corresponds to the number of measurements carried out during the analytical simulations of the debonding process. It should also be noted that in the calculation of the IAE values, the average experimental curve of each series (i.e., L50, L80 and L100) was considered. Thus, by assuming a nonlinear spring, the IAE values ranged between 6.9 % (in the L100 series) and 23.3 % (L50 series), whereas with a linear spring, the IAE values ranged between 31.4 % (L100 series) and 50.4 % (L80 series).

Fig. 11 compares the CFRP strains obtained from the analytical model and those obtained from specimen L50-T30 tested by Barris et al. [48]. From the seven reported points by Barris et al. [48], the results show, as expected, a higher CFRP strain value at the CFRP-loaded end that tends to decrease nonlinearly towards the end anchorage. From point *A* to *F*, the strains developed at the tip of the end anchorage are marginal, which means that the anchorage has not been activated so far. This can be confirmed by the load-slip curve shown in Fig. 10a, where these seven points are under the plateau corresponding to the

Table 4
Parameters for the definition of the bond-slip relationship defined in Eq. (35) for the transversely compressed end anchored CFRP-to-concrete joints tested by Barris et al. [48].

Original ID of the specimens	a (-)	b (-)	β (-)	s_t (mm)	$\tau_{b,max0}$ (MPa)	$\tau_{b,max}$ (MPa)	$\tau_{b,f}$ (MPa)
L50_T30|100|150|200	10.714	21.521	2.326	0	4.79	17.25	12.46
L80_T30|100|150|200	13.394	27.583	2.214	0	4.15	16.61	12.46
L100_T30|100|150	11.579	25.044	2.227	0	3.53	12.87	9.34

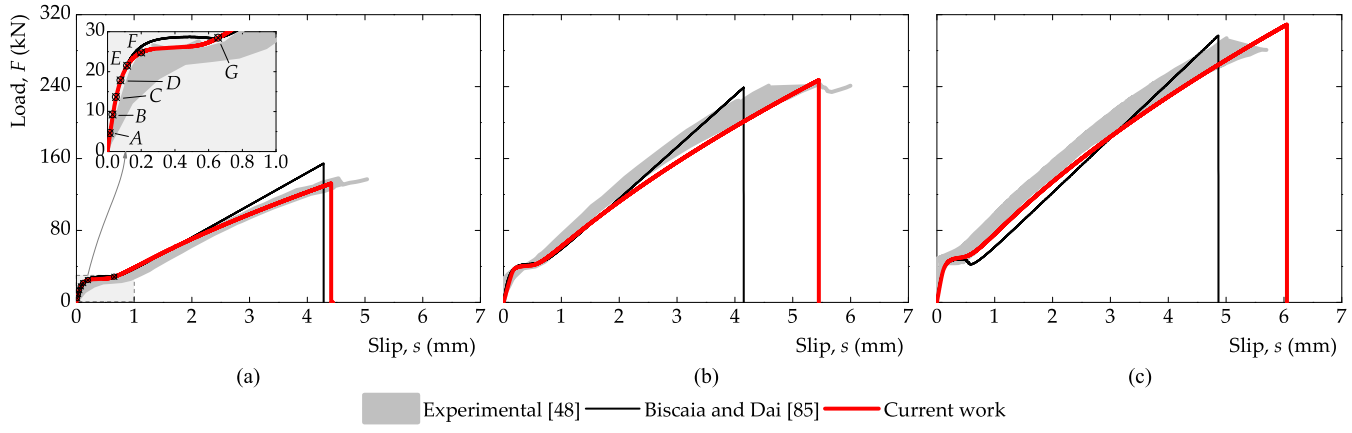

Fig. 10. Comparison between the load-slip curves obtained by the analytical model and those experimentally obtained by Barris et al. [48]: (a) when a 50 mm-wide CFRP composite was used; (b) when an 80 mm-wide CFRP composite was used; and (c) when a 100 mm-wide CFRP composite was used.

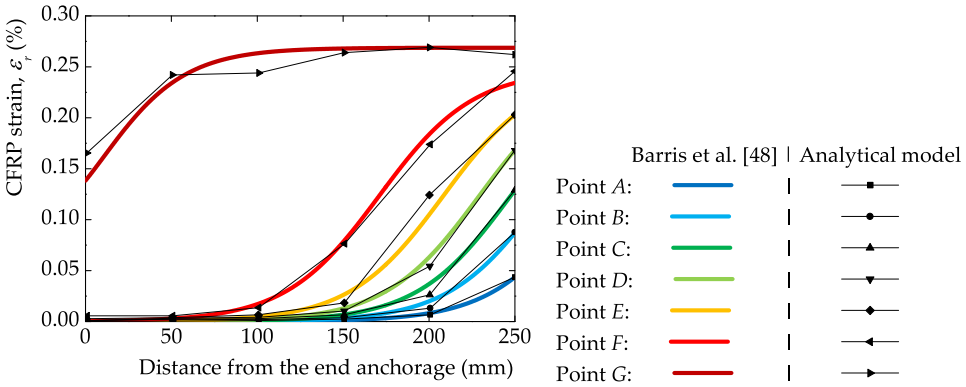

Fig. 11. Comparison between the CFRP strains obtained from the analytical model with those obtained in specimen L50-T30 [48].

CFRP-to-concrete debonding initiation. However, at point *G*, a CFRP strain of approximately 0.15 % developed at the tip of the end anchorage was measured by Barris et al. [48], as shown in Fig. 11. In this case, the influence of the transversely compressed end anchorage can be seen from the post-plateau of the load-slip curve shown in Fig. 10. Moreover, all the analytical results agree with the experimental data reported by Barris et al. [48].

5.2. Tests carried out by Codina et al. [50]

Codina et al. [50] tested a limited number of CFRP-to-concrete bonded joints with a transversely compressed anchorage in the form of a π-shape steel plate. This anchorage is 5 mm thick, 50 mm long and 140 mm wide, and it was used in three different scenarios. The first one is for reference purposes; the CFRP-to-concrete joints were free of any mechanical anchorage, and a bonded length of 250 mm was considered. In the second one, the π-shape anchorage was installed at the centre of the 250 mm bond length CFRP-to-concrete joint. In the third one, only 50 mm of the π-shape anchorage was bonded to the concrete block. Since the second scenario falls outside the conditions of the analytical model, only the other two scenarios were considered here.

Briefly, a 1.4 mm thick CFRP strip with 50 mm width was bonded onto a concrete block with 200 × 200 × 370 mm (thickness × width × length). The mechanical properties of the CFRP were not tested, and the values reported by the fabricant were considered, i.e., an elastic modulus of 170 GPa, a rupture strain of 1.60 % and a tensile strength of 2800 MPa. To determine the mechanical properties of the concrete, the compression tests of three cylinders led to an average strength of 45.98 MPa and an elastic modulus of 36.21 GPa. The S&P Resin 220 HP was used, which is the same resin used by Aghabagloo et al. [89].

As for the local bond-slip relationship, Codina et al. [50] suggested a bond-slip relationship with a triangular shape for the EBR specimen, whereas a triangular shape with a residual bond stress was obtained for the HB specimen. Thus, for the EBR specimen, a maximum shear bond stress of 12.70 MPa with a corresponding maximum slip of 0.030 mm and a final slip, i.e., beyond which the CFRP completely separates from the concrete, of 0.180 mm was reported by Codina et al. [50]. The fracture energy associated with this EBR specimen is 1.143 N/mm. In the case of the HB specimen, the same maximum shear bond stress and maximum slip were reported. However, from a slip of 0.400 mm on, a friction stress of 7.40 MPa was obtained by Codina et al. [50]. The exponential bond-slip relationship in Eq. (8) was approximated, through the least square minimisation process, to the triangular bond-slip relationship, whilst Eq. (35) was used to approximate the bond-slip relationship of the HB specimen. In both cases, the maximum shear bond stress and the fracture energy were set as constraints in the minimisation process. However, since the HB specimen has a short length, an average shear bond stress was considered and determined from the load-slip curve. Therefore, a maximum shear bond stress of 11. 54 MPa and a residual bond stress of 7.60 MPa were considered in that minimisation process. Thus, the stiffness index in Eq. (8) was set equal to $B = 21.796\ \text{mm}^{-1}$, whilst the parameters in Eq. (35) were set equal to $a = 13.241$, $b = 29.453$, $\beta = 1.035$, and $s_t = 0.356$ mm.

It should also be noted that these experimental results do not follow the Mohr-Coulomb failure criterion. This is because, on the HB specimen, not only did the authors [50] bond the CFRP to the concrete block, but they also bonded the steel plate to the CFRP composite. Therefore, the two bonded interfaces (i.e., steel-to-CFRP and CFRP-to-concrete) contributed to the final improvement of the HB specimen but avoided a fair comparison between specimens through the use of the

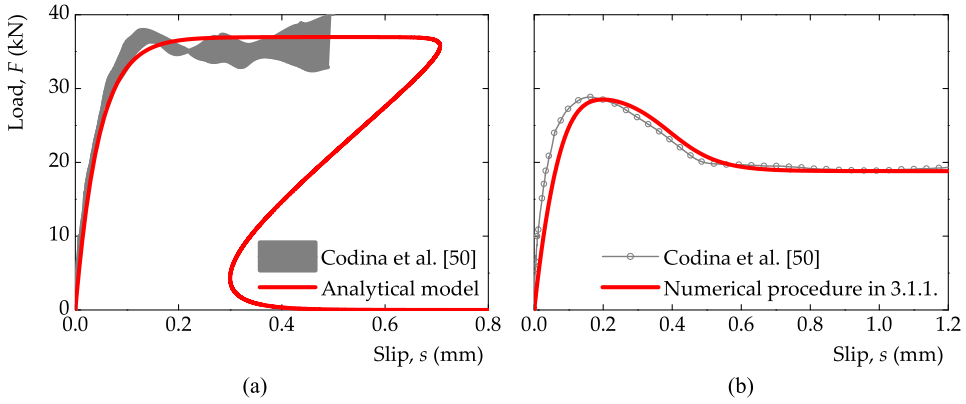

Fig. 12. Comparison between the load-slip curves obtained by Codina et al. [50] and: (a) by the analytical model for the specimens with a bonded length of 250 mm and free of any mechanical anchorage; and (b) by the numerical procedure described in Subsection 3.1.1 for the specimen with only a 50 mm long end anchorage.

Mohr-Coulomb failure criterion.

Fig. 12 shows the results obtained from the analytical model (EBR) and the numerical procedure discussed in Subsection 3.1.1. The analytical load-slip curve shown in Fig. 12a has good agreement with the experimental result. The plateau at maximum load can be seen in both load-slip curves and, in the case of the analytical model, it occurs at 37.0 kN, which is approximately 5.8 % lower than the average maximum load of 39.2 kN determined by Codina et al. [50]. Fig. 12b compares the load-slip curve of the mechanically anchored CFRP-to-concrete joint obtained by the numerical procedure described in Subsection 3.1.1 with that which was experimentally obtained by Codina et al. [50]. Once again, these predicted results are fairly consistent with the experiments. In this case, the maximum loads in both situations are similar, i.e. 28.5 kN in the numerical simulation and 28.8 kN reported by Codina et al. [50]. The same proximity can be found for the frictional load, where approximately 18.8 kN was obtained in both cases.

Due to the absence of further reliable data and following the same rationale of the studied specimens described in Subsection 3.2, four more CFRP-to-concrete specimens with a transversely compressed end anchorage were idealised. Thus, the same 50 mm long end anchorage and another with 260 mm long were assumed. As a bonded length, 50 mm and 260 mm were also considered. To allow the use of the Mohr-Coulomb failure criterion, the bond-slip relationship of the EBR specimen was used as a reference for the definition of the bond-slip relationship of the HB specimen, where the steel plate is not bonded to the CFRP composite. The corresponding load-slip curves of these idealised specimens are shown in Fig. 13. Like the specimens previously analysed in Subsection 3.2, the results show that using a short-end anchorage leads to a smaller increase in the load capacities of the specimens and a more meaningful load increment with the use of the 260 mm long-end anchorage. The ductility of the specimens with the longest end anchorage is also improved and is higher when the CFRP-to-concrete joints have a bonded length of 260 mm.

Since Codina et al. [50] have reported reliable experimental data with a π-shape anchorage installed at the centre of the CFRP-to-concrete joint with a total bonded length of 250 mm, this case was compared with its use as an end anchorage of the same CFRP-to-concrete joint. Thus, Fig. 14 compares the experimental and analytical load-slip curves reported by Codina et al. [50] with those obtained by the analytical model in which the π-shape anchorage is installed at the CFRP unloaded end. The load-slip curves in Fig. 14 show that using the end anchorage does not have the same load improvement as when the π-shape anchorage is installed at the centre of the CFRP-to-concrete joint. Moreover, when compared with the EBR specimens, and unlike the use of the anchorage installed at the centre of the CFRP-to-concrete joint, the maximum load

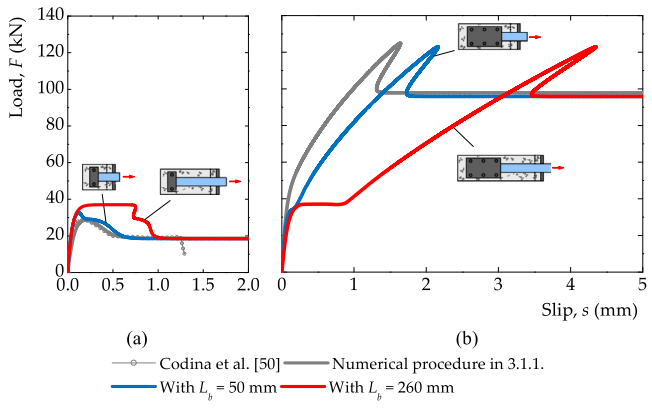

Fig. 13. Influence on the load-slip curve on the CFRP-to-concrete joint when: (a) a 50 mm long end anchorage described by Codina et al. [50] is used; and (b) a 260 mm long end anchorage with the same bond characteristics as the 50 mm long end anchorage described by Codina et al. [50] is used.

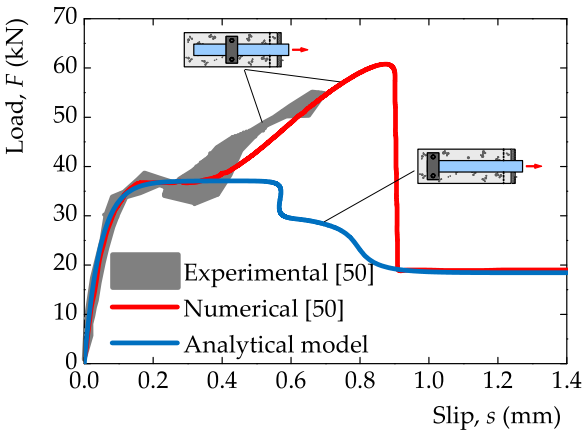

Fig. 14. Influence of the place where the anchorage used by Codina et al. [50] is installed along the CFRP-to-concrete bonded joint.

was not improved, which means that using the end anchorage is, in this case, completely inefficient. Despite being out of the scope of the present work, these results open a new discussion that requires further studies so that the influence of the place where the mechanical anchorage should be installed can be better understood.

5.3. *Tests carried out by Gao et al. [49]*

Gao et al. [49] carried out an experimental program to evaluate the bond behaviour between CFRP sheets and concrete. The authors [49] analysed the bond characteristics of seven specimens tested under the single-shear test. The bond characteristics of the CFRP-to-concrete joints with mechanical fastenings, similar to a π-shape, were also considered, and the bond-slip relationships with and without the influence of the mechanical fastenings were obtained. Four CFRP plies, each with a nominal thickness of 0.167 mm and 50 mm wide, were EB to a concrete block with a cross-sectional area of 250 × 180 mm (width × thickness). The elastic modulus of the CFRP is 250 GPa with a rupture strain of 1.80 %. The mechanical properties of the concrete were determined after 28 days of curing and leding to a mean strength of 59 MPa and an elastic modulus of 34.5 GPa. The authors [49] used Sikadur-300 epoxy resin to impregnate the carbon sheets as well as to promote the adhesion between the CFRP and the concrete block. The mechanical fasteners were made of rectangular thin steel plates measuring 120 × 60 × 5 mm (width × length × thickness), and each fastener was installed with the help of two chemical 8 mm diameter bolts by applying a 15 N·m torque. Two and three mechanical fasteners were used on CFRP-to-concrete bonded joints with bonded lengths of 730 mm and 1230 mm, respectively. For reference purposes, a set of specimens was also tested with no mechanical fasteners at all.

Although these tests do not completely fall into the subject covered by this work, the authors [49] have reported the bond-slip relationships of the CFRP-to-concrete joints with and without the influence of the mechanical fasteners. They approximated the local bond behaviour of the CFRP-to-concrete joints free of any mechanical anchorage to an exponential bond-slip relationship similar to that defined in Eq. (8). For the definition of the bond-slip relationship of the mechanically anchored CFRP-to-concrete joints, the authors [49] adapted the original proposal made by Biscaia et al. [45], which allowed them to reproduce the friction state of the joint. So, the bond-slip relationships defined in Eqs. (8) and (32) were both approximated to the bond-slip relationships reported by Gao et al. [49] through the same minimisation process described above. As a result, the bond-slip relationship of the specimens without mechanical fasteners was defined as follows: $\tau_{b,\max} = 4.41$ MPa, $B = 7.109$ mm^{-1}, and $G_F = 1.239$ N/mm. On the other hand, all the parameters needed to define the bond-slip relationship of the mechanically

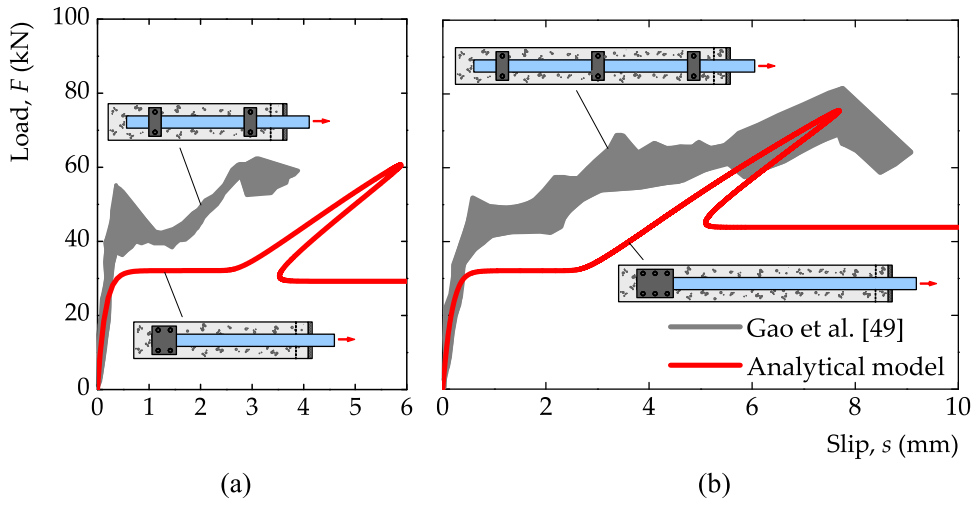

Fig. 15. Load-slip curves obtained by the analytical model and by Gao et al. [49]: (a) comparison between the use of an end anchorage with 2 π-shape anchorages with the same length; and (b) comparison between the use of an end anchorage with 3 π-shape anchorages with the same length.

anchored CFRP-to-concrete joints are $\tau_{b,\max} = 9.43$ MPa, $\tau_{b,f} = 5.02$ MPa, $a = 7.654$, $b = 16.219$, $\beta = 3.125$, and $s_t = 7.483 \times 10^{-5}$ mm. Like the specimens analysed in Subsection 3.2, a friction angle of 1.0 rad was assumed, which, considering the Mohr-Coulomb failure criterion, means that a compressive stress of 3.22 MPa was applied to the mechanical fasteners. As in the work of Codina et al. [50], where the Mohr-Coulomb failure criterion did not accurately represent the CFRP-to-concrete joints with the transversely compressed end anchorage due to the additional adhesion between the steel plate and the CFRP composite, in this case, the same double interfaces (steel--to-CFRP and CFRP-to-concrete) were created beneath the end anchorage.

Fig. 15 shows the results obtained from the analytical model. In Fig. 15a, the experimental load-slip curves obtained by Gao et al. [49] correspond to the case where two mechanical fasteners placed 500 mm apart were considered, while Fig. 15b shows the load-slip curves where three mechanical fasteners were used and also placed at intervals of 500 mm. For fair comparisons, the length of the end anchorages was kept the same, i.e., in the case of the CFRP-to-concrete joints with two mechanical fasteners, the length of the end anchorage is 120 mm and in the other case with three mechanical fasteners, a 180 mm long end anchorage was considered. Comparing the analytical results obtained from the CFRP-to-concrete joint with an end anchorage with the experimental data obtained by Gao et al. [49], it can be seen that the load capacities of the CFRP-to-concrete joints with the mechanical fasteners are greater than those obtained from the CFRP-to-concrete joints with an end anchorage. These results are consistent with those obtained in the previous subsection.

6. Conclusions

An analytical model was proposed to simulate the bond performance of FRP composites externally bonded to a substrate with a transversely compressed mechanical end anchorage. A series of different CFRP-to-substrate joints was considered, and the debonding process was simulated with the FEM. The analytical model was also used to simulate some experimental tests found in the literature. Hence, from all the results reported in this study, the following main conclusions can be enumerated:

- The wide applicability of the analytical model in predicting the bond performance of FRP-to-substrate joints was shown. Good accuracy with the numerical results obtained from the FEM was also shown, which allowed us to validate the analytical model;
- Once the nonlinear load-slip relationship of the transversely compressed end anchorage is known, the analytical model can be used to predict the complete debonding process of the mechanically anchored FRP-to-substrate joints. It is also applicable to cases without end anchorages;
- To obtain the nonlinear load-slip relationship, two different numerical procedures can be used. The first, which is more complex, allows us to capture the snap-back phenomenon associated with the FRP-to-substrate joints with a long totally bonded length. The second one, which is a much simpler numerical procedure, can be used only for long FRP-to-substrate joints, and it fails to capture the complete debonding of the joint, and only accounts for the FRP rupture;
- The use of short-end anchorages is not efficient since they cannot significantly increase the load capacities of FRP-to-substrate joints. However, when the same compressive stresses used on the short anchorages were applied to longer end anchorages, meaningful improvements in the load capacities of the joints were reached. When the same load is applied, the long-end anchorage leads to higher load capacities and ductility than the short-end anchorage;
- The analytical model, when confronted with the reliable data found in the literature, reproduces the debonding process accurately. It was also more accurate than the predictions made by assuming a linear behaviour for the end anchorage;
- Despite being out of the scope of the present work, a comparison between CFRP-to-concrete bonded joints that are mechanically anchored with several-shape fasteners and those utilising an equivalent end anchorage, i.e., with the same anchorage length as the π-shape fasteners, suggested that the shape could lead to higher load capacities. This presents an opportunity for further exploration and study in the future, where the developed analytical model can serve as a basis for comparison.

CRediT authorship contribution statement

Jian-Guo Dai: Writing – review & editing, Validation, Investigation. **Cristina Barris:** Writing – review & editing, Validation, Investigation. **Biscaia Hugo C:** Writing – original draft, Validation, Software, Project administration, Methodology, Investigation, Funding acquisition, Formal analysis, Data curation, Conceptualization.

Declaration of Competing Interest

The authors declare the following financial interests/personal relationships which may be considered as potential competing interests:

Hugo C. Biscaia reports financial support was provided by Foundation for Science and Technology.

Acknowledgments

The first author is thankful to Fundação para a Ciência e Tecnologia (FCT-MCTES) for the partial funding of this work under the strategic project UID/00667: Unidade de Investigação e Desenvolvimento em Engenharia Mecânica e Industrial (UNIDEMI).

References

[1] Bambach MR, Elchalakani M, Zhao XL. Composite steel–CFRP SHS tubes under axial impact. Compos Struct 2009;87(3):282–92.
[2] Suvarna R, Arumugam V, Bull DJ, Chambers AR, Santulli C. Effect of temperature on low velocity impact damage and post-impact flexural strength of CFRP assessed using ultrasonic C-scan and micro-focus computed tomography. Compos Part B Eng 2014;66:58–64.
[3] Mhanna HH, Hawileh RA, Abdalla JA. Shear strengthening of reinforced concrete beams using CFRP wraps. Procedia Struct Integr 2019;17:214–21.
[4] Daniyan IA, Mpofu K, Adeodu AO, Adesina O. Development of carbon fibre reinforced polymer matrix composites and optimization of the process parameters for railcar applications. Mater Proc 2021;38(2):628–34.
[5] Zhang B, Zhu H, Yang Z, Dong YR. BFRP bars reinforced geopolymer-based coral aggregate concrete beams with sustainable and high seawater erosion resistance: flexural durability, economic, and ecological analysis. Eng Struct 2025;330:11991.
[6] Tehrani BN, Mostofinejad D, Hosseini SM. Experimental and analytical study on flexural strengthening of RC beams via prestressed EBROG CFRP plates. Eng Struct 2019;197:109395.
[7] Ghahsareh FM, Mostofinejad D. Groove classification in EBROG FRP-to-concrete joints. Constr Build Mater 2021;275:122169.
[8] Sanginabadi K, Yazdani A, Mostofinejad D, Czaderski C. RC members externally strengthened with FRP composites by grooving methods including EBROG and EBRIG: a state-of-the-art review. Constr Build Mater 2022;324:126662.
[9] Ghaleh RZ, Mostofinejad D. Behaviour of EBRIG CFRP sheet-concrete joint: comparative assessment with EBR and EBROG methods. Constr Build Mater 2022;346:128374.
[10] Shomali A, Mostofinejad D, Esfahani MR. Shear strengthening of RC beams using EBRIG CFRP strips: a comparative study. Eur J Environ Civ Eng 2021;25:14.
[11] Wu G, Dong ZQ, Wu ZS, Zhang LW. Performance and parametric analysis of flexural strengthening for RC beams with NSM-CFRP bars. J Compos Constr 2013;18(4).
[12] Zhang SS, Yu T, Chen GM. Reinforced concrete beams strengthened in flexure with near-surface mounted (NSM) CFRP strips: current status and research needs. Compos Part B Eng 2017;131:30–42.
[13] Barris C, Sala P, Gómez J, Torres L. Flexural behaviour of FRP reinforced concrete beams strengthened with NSM CFRP strips. Compos Struct 2020;241:112059.
[14] Abdallah M, Al-Mahmoud F, Tabet-Derraz MI, Khelil A, Mercier J. Experimental and numerical investigation on the effectiveness of NSM and side-NSM CFRP bars for strengthening continuous two-span RC beams. J Build Eng 2021;41:102723.
[15] Biscaia H, Chastre C, Cruz D, Franco N. Flexural strengthening of old timber floors with laminated carbon fiber reinforced polymers. J Compos Constr 2017;20(1):04016073.
[16] Franco N, Chastre C, Biscaia H. Strengthening RC beams using stainless-steel continuous reinforcement embedded at ends. J Struct Eng 2020;146(5):04020065.
[17] Azevedo A, Firmo J, Correia J, Chastre C, Biscaia H, Franco N. Fire behaviour of CFRP-strengthened RC slabs using different techniques - EBR, NSM and CREatE. Compos Part B Eng 2022;230:109471.
[18] Llauradó PV, Ibell T, Gómez JF, Ramos FJG. Pull-out and shear-strength models for FRP spike anchors. Compos Part B Eng 2017;116:239–52.
[19] Li Weiwen, Liu Wei, Yang Xu, Xing Feng. Experimental study on FRP-to-concrete bonded joints with FRP sheet anchor system. Adv Mater Sci Eng 2020;2020:2514313.
[20] Sun W, Liu S, Zhang C. An effective improvement for enhancing the strength and feasibility of FRP spike anchors. Compos Struct 2020;247:112449.
[21] Alshami GS, Hawileh RA, Tatar J, Abdalla JA. Influence of CFRP spike anchors on the performance of flexural CFRP sheets externally bonded to concrete. J Compos Constr 2023;27(5).
[22] Al-Mahaidi R, Kalfat R. Investigation into CFRP laminate anchorage systems utilising bi-directional fabric wrap. Compos Struct 2011;93(4):1265–74.
[23] Al-Mahaidi R, Kalfat R. Investigation into CFRP plate end anchorage utilising uni-directional fabric wrap. Compos Struct 2011;93(2):821–30.
[24] Haddad RH, Marji CS. Composite strips with U-shaped CFRP wrap anchor systems for strengthening reinforced concrete beams. Int J Civ Eng 2019;17:1799–811.
[25] Tatar J, Viniarski C, Ishfaq M, Harries KA, Head M. Effect of U-wrap anchors on flexural behavior of reinforced concrete beams flexurally strengthened with externally bonded CFRP sheets. J Compos Constr 2022;27(1).
[26] Biscaia HC, Micaelo R, Teixeira J, Chastre C. Numerical analysis of FRP anchorage zones with variable width. Compos Part B Eng 2014;67:410–26.
[27] Biscaia H, Micaelo R. Emerging anchored FRP systems bonded to steel subjected to monotonic and cyclic loading: a numerical study. Eng Fract Mech 2022;261:108250.
[28] Realfonzo R, Martinelli E, Napoli A, Nunziata B. Experimental investigation of the mechanical connection between FRP laminates and concrete. Compos Part B Eng 2013;45(1):341–55.
[29] Kopraman Y, Özdemir A, Anıl Ö, Sakin S, Armakan F. Experimental investigation of bond–slip behaviour of between-anchored steel strips to concrete surface. Arch Civ Mech Eng 2022;22:198.
[30] Narmashiri K, Jumaat MZ, Sulong NHR. Investigation on end anchoring of CFRP strengthenedsteel I-beams. Int J Phys Sci 2010;5(9):1360–71.
[31] Zhou Y, Wang X, Sui L, Xing F, Huang Z, Chen C, Li P, Me L. Effect of mechanical fastening pressure on the bond behaviors of hybrid-bonded FRP to concrete interface. Compos Struct 2018;204:731–44.
[32] Gao L, Wei Q, Huang Y, Zhang F. Influence of anchor design parameters on flexural performance of hybrid bonded-fiber reinforced polymer strengthened reinforced concrete beams. Structures 2023;48:1029–45.
[33] Alkhateeb MY, Hejazi F. Reinforced concrete beams externally strengthened by CFRP rods with steel plate, anchorage bolts, and concrete jacketing. Structures 2022;46:1994–2013.
[34] Yuan H, Teng JG, Seracino R, Wu ZS, Yao J. Full-range behavior of FRP-to-concrete bonded joints. Eng Struct 2004;26(5):553–65.
[35] Mazzotti C, Savoia M, Ferracuti B. An experimental study on delamination of FRP plates bonded to concrete. Constr Build Mater 2008;22(7):1409–21.
[36] Fernando D, Yu T, Teng JG. Behavior of CFRP laminates bonded to a steel substrate using a ductile adhesive. J Compos Constr 2013;18(2):04013040.
[37] Biscaia HC, Chastre C, Viegas A. A new discrete method to model FRP–to-parent material bonded joints. Compos Struct 2015;121:280–95.
[38] Biscaia HC, Borba IS, Silva C, Chastre C. A nonlinear analytical model to predict the full-range debonding process of FRP-to-parent material interfaces free of any mechanical anchorage devices. Compos Struct 2016;138:52–63.
[39] Kalfat R, Smith ST. Anchorage devices used to improve the performance of reinforced concrete beams retrofitted with FRP composites: state-of-the-art review. J Compos Constr 2013;17:14–33.
[40] Michels J, Martinelli E, Czaderski C, Motavalli M. Prestressed CFRP strips with gradient anchorage for structural concrete retrofitting: experiments and numerical modelling. Polymers 2014;6:114–31.
[41] Correia L, Barris C, França P, Sena-Cruz J. Effect of temperature on bond behavior of externally bonded FRP laminates with mechanical end anchorage. J Compos Constr 2019;23(5):04019036.
[42] Wang Y, Huang C, Guo X. Study on the influence of end anchoring on CFRP-concrete interface through double-lap shear testing. Structures 2024;69:107457.
[43] Wang Y, Guo X, Bai J. An analytical model to predict bond behavior of fiber reinforced polymer bonded to concrete with an end anchorage system. J Reinf Plast Compos 2023;43(9–10):469–83.
[44] Hansen CS, Schmidt JW, Stan H. Transversely compressed bonded joints. Compos Part B Eng 2012;43(2):691–701.
[45] Biscaia HC, Chastre C, Silva MAG. Bond-slip model for FRP-to-concrete bonded joints under external compression. Compos Part B Eng 2015;80:246–59.
[46] Biscaia H, Chastre C. Design method and verification of steel plate anchorages for FRP-to-concrete bonded interfaces. Compos Struct 2018;192:52–66.
[47] Dai JG, Ueda T, Sato Y. Development of the nonlinear bond stress-slip model of fiber reinforced plastics sheet-concrete interfaces with a simple method. J Compos Constr 2005;9(1):52–62.
[48] Barris C, Correia L, Sena-Cruz J. Experimental study on the bond behaviour of a transversely compressed mechanical anchorage system for externally bonded reinforcement. Compos Struct 2018;200:217–28.
[49] Gao L, Zhang F, Liu J, Lu X, Gao H. Experimental and numerical study on the interfacial bonding characteristics of FRP-to-concrete joints with mechanical fastening. Constr Build Mater 2019;199:456–70.
[50] Codina A, Torres L, D'Antino T, Baena M, Barris C. Flexural performance of RC beams strengthened with HB CFRP plates: experimental study and theoretical model based on the intermediate crack debonding. Constr Build Mater 2025;458:139444.
[51] Wang G, Chen T, Cao C, Zheng Y. Strip-based numerical analysis of CFRP-reinforced steel plates with multiple debonding defects using the Runge-Kutta method. Compos Struct 2024;337:118059.
[52] Yang Y, Zhao J, Zhang S, Chastre C, Biscaia H. Effect of mechanical anchorage on the bond performance of double overlapped CFRP-to-steel joints. Compos Struct 2021;267:113902.
[53] Zhang SS, Ke Y, Chen E, Biscaia H, Li WG. Effect of load distribution on the behaviour of RC beams strengthened in flexure with near-surface mounted (NSM) FRP. Composite Structures 2022;279:114782.
[54] Lu T, Li P, Cui C, Wu J, Fu B. Shear transferring mechanism of the FPR-to-concrete bonded joint with end U-jacketing: a theoretical study. Structures 2023;56:104991.
[55] Caggiano A, Martinelli E, Faella C. A fully-analytical approach for modelling the response of FRP plates bonded to a brittle substrate. Int J Solids Struct 2012;49(17):2291–300.
[56] Gao WY, Dai JG, Teng JG. Analysis of mode II debonding behavior of fiber-reinforced polymer-to-substrate bonded joints subjected to combined thermal and mechanical loading. Eng Fract Mech 2015;136:241–64.
[57] Yang Y, Biscaia H, Chastre C, Silva MAG. Bond characteristics of CFRP-to-steel joints. J Constr Steel Res 2017;138:401–19.

[58] Nelson LA, Al-Allaf M, Weekes L. Analytical modelling of bond-slip failure between epoxy bonded FRP and concrete substrate. Compos Struct 2020;251:112596.
[59] Milani G, Grande E, Bertolesi E, Rotunno T, Fagone M. Debonding mechanism of FRP strengthened flat surfaces: analytical approach and closed form solution. Constr Build Mater 2021;302:124144.
[60] Biscaia HC, Chastre C, Borba IS, Silva C, Cruz D. Experimental evaluation of bonding between CFRP laminates and different structural materials. J Compos Constr 2016;20(3):04015070.
[61] He J, Xian G, Zhang YX. Numerical modelling of bond behaviour between steel and CFRP laminates with a ductile adhesive. Int J Adhes Adhes 2021;104:102753.
[62] Zhao J, Fang J, Yang Y, Zhang S, Biscaia H. Experimental study on mixed mode-I & II bond behavior of CFRP-to-steel joints with a ductile adhesive. ThinWalled Struct 2023;184:110532.
[63] Biscaia H, Coelho P, Conde F, D'Antino T. Theoretical study on the bond performance of CFRP-to-steel single-lap shear tests with multiple debonding defects. Compos Struct 2024;345:118406.
[64] Biscaia H, Franco N, Chastre C. Stainless steel bonded to concrete: an experimental assessment using the DIC technique. Int J Concr Struct Mater 2018;12(9).
[65] He J, Xian GJ. Debonding of CFRP-to-steel joints with CFRP delamination. Compos Struct 2016;153:12–20.
[66] Biscaia HC, Chastre C, Silva MAG. Analytical model with uncoupled adhesion laws for the bond failure prediction of curved FRP-concrete joints subjected to temperature. Theor Appl Fract Mech 2017;89:63–78.
[67] Wang HT, Wu G. Bond-slip models for CFRP plates externally bonded to steel substrates. Compos Struct 2018;184:1204–14.
[68] Biscaia H, Franco N, Chastre C. Development of a simple bond-slip model for joints monitored with the DIC technique. Arch Civ Mech Eng 2018;18(4):1535–46.
[69] Pang Y, Wu G, Wang H, Gao D, Zhang P. Bond-slip model of the CFRP-steel interface with the CFRP delamination failure. Compos Struct 2021;256:113015.
[70] Cornetti P, Carpinteri A. Modelling the FRP-concrete delamination by means of an exponential softening law. Eng Struct 2011;33(6):1988–2001.
[71] Zhang SS, Teng JG, Yu T. Bond-slip model for CFRP strips near-surface mounted to concrete. Eng Struct 2013;56:945–53.
[72] Mukhtar FM, Shehadah ME. Experimental verification of 2- and 3-D numerical models for bond-slip behavior of CFRP-concrete. Constr Build Mater 2021;287:122814.
[73] Zhang F, Gao L, Wei Q. Theoretical and numerical bonding capacity model of FRP-to-concrete joints with mechanical fastening. Constr Build Mater 2022;353:129066.
[74] Nelson LA, Weekes L, Milani G, Al-Allaf M. Generalised analytical solutions for linear and non-linear bond-slip models for externally bonded FRP to a concrete substrate. Eng Struct 2024;298:117025.
[75] Yang Y, Silva MAG, Biscaia H, Chastre C. Bond durability of CFRP laminates-to-steel joints subjected to freeze-thaw. Compos Struct 2019;212:243–58.
[76] Li A, Wang H, Li H, Kong D, Xu S. Estimation of bond strength and effective bond length for the double strap joint between carbon fiber reinforced polymer (CFRP) plate and corroded steel plate. Polymers 2022;14:3069.
[77] Biscaia HC, Ribeiro P. A temperature-dependent bond-slip model for CFRP-to-steel joints. Compos Struct 2019;217:186–205.
[78] Vaculik J, Visintin P, Burton NG, Griffith MC, Seracino R. State-of-the-art review and future research directions for FRP-to-masonry bond research: test methods and techniques for extraction of bond-slip behaviour. Constr Build Mater 2018;183:325–45.
[79] Zhang D, Yang J, Chi LY. The bond-slip relationship at FRP-to-brick interfaces under dynamic loading. Materials 2021 2021;14(3):545.
[80] Biscaia HC. The influence of temperature variations on adhesively bonded structures: a non-linear theoretical perspective. Int J NonLinear Mech 2019;113:67–85.
[81] Biscaia HC, Canejo J, Zhang S, Almeida R. Using digital image correlation to evaluate the bond between carbon fibre-reinforced polymers and timber. Struct Health Monit 2021:1–24.
[82] Biscaia HC, Chastre C, Silva C, Franco N. Mechanical response of anchored FRP bonded joints: a nonlinear analytical approach. Mech Adv Mater Struct 2018;25(3):238–52.
[83] Zhou H, Yang Y, Liu K, Huang T, Ou Y, Zhang SS. Analytical study on the behavior of CFRP-concrete bonded joint with a non-rigid end-anchor. Compos Struct 2023;326:117609.
[84] Biscaia H, D'Antino T, Coelho P, Conde F. Influence of multiple debonding defects on the behaviour of mechanically anchored CFRP-to-steel joints. Compos Struct 2025;355:118847.
[85] Biscaia H, Dai JG. An innovative wide-ranging analytical approach for modelling the bond behaviour of FRP-to-substrate joints with an elastic end anchorage. Eng Fract Mech 2025;313:110662.
[86] Jiang C, Yu QQ, Gu XL. A unified bond-slip model for the interface between FRP and steel. Compos Part B Eng 2021;227:109380.
[87] Biscaia H, Carmo N. Bond assessment between rebars embedded into a parent material using a single-function bond-slip model. Constr Build Mater 2023;397:132396.
[88] S&P. S&P Resin 220 HP Epoxy Adhesive (2019), Technical Data Sheet; S&P: Seewen, Switzerland.
[89] Aghabagloo M, Carreras L, Barris C, Codina A, Baena M. Interfacial behavior of hybrid-bonded CFRP-to-concrete joints. Procedia Struct Integr 2024;64:1516–23.
[90] S&P. S&P CFRP Laminate (2017), Technical Datasheet; S&P: Seewen, Switzerland.
[91] Biscaia HC, Chastre C, Silva MAG. A smeared crack analysis of reinforced concrete T-beams strengthened with GFRP composites. Eng Struct 2013;56:1346–61.
[92] Biscaia HC, Chastre C, Silva MAG. Modelling GFRP-to-concrete joints with interface finite elements with rupture based on the Mohr-Coulomb criterion. Constr Build Mater 2013;47:261–73.
[93] Biscaia HC, Chastre C, Silva MAG. Double shear tests to evaluate the bond strength between GFRP/concrete elements. Compos Struct 2012;94(2):681–94.
[94] Biscaia HC, Micaelo R, Chastre C. Cyclic performance of adhesively bonded joints using the distinct element method: damage and parametric analysis. Compos Part B Eng 2019;178:107468.
[95] Biscaia HC, Micaelo R, Cornetti P, Almeida R. Numerical bond assessment of carbon-epoxy stepped-lap joints. Eng Fract Mech 2023;289:109413.
[96] Rozylo P, Falkowicz K. Stability and failure analysis of compressed thin-walled composite structures with central cut-out, using three advanced independent damage models. Compos Struct 2021;273:114298.
[97] Rozylo P, Debski H. Failure study of compressed thin-walled composite columns with top-hat cross-section. ThinWalled Struct 2022;180:109869.
[98] Cervenka V., Jendele L., Cervenka J. ATENA Program Documentation – Part 1 – Theory. Cervenka Consulting, Prague, March, 2021.
[99] Biscaia HC. Closed-form solutions for modelling the response of adhesively bonded joints under thermal loading through exponential softening laws. Mech Mater 2020;148:103527.
[100] Popovics S. A numerical approach to the complete concrete stress-strain relation for concrete. Cem Concr Res 1973;3(5):583–99.
[101] Wu YF, Zhao XM. Unified bond stress-slip model for reinforced concrete. J Struct Eng 2013;139(11):1951–62.
[102] Shen D, Shi X, Ji Y, Yin F. Strain rate effect on bond stress-slip relationship between basalt fiber-reinforced polymer sheet and concrete. J Reinf Plast Compos 2015;34(7):547–63.